Research Square

Preprints are preliminary reports that have not undergone peer review.
They should not be considered conclusive, used to inform clinical practice,
or referenced by the media as validated information.

Optimization of Hydrothermal Enhancement in Outwardly Corrugated Pipes of Heat Exchanger

Sunday Chukwuka Iweka

chukaiweka@yahoo.com

Southern Delta University, Ozoro

Henry Freedom Ifowodo

Southern Delta University, Ozoro

ALfred .O Emu

Southern Delta University, Ozoro

Sylvester Chukwuktem Onwusa

Southern Delta University, Ozoro

Research Article

Keywords: Heat Exchanger, Convective Heat Transfer, Outwardly Corrugated Pipes, Hydrothermal Performance

Posted Date: October 30th, 2026

DOI: https://doi.org/10.21203/rs.3.rs-11354502/v1

License: This work is licensed under a Creative Commons Attribution 4.0 International License.
Read Full License

Additional Declarations: No competing interests reported.

Optimization of Hydrothermal Enhancement in Outwardly Corrugated Pipes of Heat Exchanger

Sunday Chukwuka Iweka[1*], Henry Freedom Ifowodo[2], Alfred .O. Emu[3], Sylvester Chukwutem Onwusa[4]

[1,4]Department of Mechanical Engineering, Southern Delta University, Ozoro, Nigeria.

[2]Department of Industrial and Production Engineering, Southern Delta University, Ozoro, Nigeria.

[3]Department of Marine Engineering, Southern Delta University, Ozoro, Nigeria.

[*]Corresponding Author email: iwekasc@sdu.edu.ng, chukaiweka@yahoo.com

Abstract

In this study, we numerically investigated the turbulence convective heat transfer performance (CHTP) and entropy production rate (EPR) of distilled water flowing through outwardly corrugated pipes. The effects of Reynolds number ($5.0 \times 10^3 \leq Re \leq 4.0 \times 10^4$), normalized corrugation amplitude ($0.03 \leq e/D \leq 0.05$), and normalized pitch ($0.9 \leq P/D \leq 1.1$) on the average Nusselt number (Nu), friction factor(fr), performance evaluation criterion(PEC), field synergy number(FSN), and volumetric entropy production rate were examined. The results show that corrugation significantly improves heat transfer relative to the smooth pipe. Over the full Reynolds number range, Nu increased by factors of 5.98, 5.19, and 4.81 for the same amplitude values, while the corresponding PEC remained above unity, indicating an overall thermal-hydraulic advantage. The findings demonstrate that, in comparison to smooth pipe, corrugation enhances heat transfer performance. Stronger wall-induced secondary motion enhances the alignment between velocity and temperature-gradient fields, as evidenced by the field synergy number increasing with increasing corrugation amplitude but decreasing with increasing Reynolds number and pitch. A new term called synergy-thermal coupling index (STC) was introduced to evaluate how effectively field synergy translates into heat transfer enhancement. The STC analysis demonstrated that the improvement in convective heat transfer cannot be exclusively attributed to improved synergy between velocity and temperature gradient, as part of the gain is also associated with recirculation and turbulence production. In addition, multi-objective optimization revealed a clear trade-off among thermal enhancement, frictional drawback, and entropy generation, with the Pareto front indicating that the most favourable operating region occurs at a relatively low Reynolds number and moderate corrugation intensity.

Keywords: *Heat Exchanger; Convective Heat Transfer; Outwardly Corrugated Pipes; Hydrothermal Performance.*

1.0. Introduction

Forced internal convective heat transfer is an essential transport process in many heat systems, including heat exchangers, automotive components, electronic cooling systems, air conditioning units, and solar heat collectors [1, 2]. In such systems, thermal performance is controlled by the interaction between the coolant's motion and heat transfer between the wall and the coolant [3]. Due to its strong practical importance, convective heat transfer in internal flows has been extensively investigated, especially in circular smooth pipes, which remain common in engineering applications because of their simplicity, ease of construction, and ease of inspection [4]. However, smooth pipes are associated with relatively low heat transfer rates, which has stimulated a continued interest in passive heat transfer enhancement techniques [5, 6].

Passive methods are generally simpler, more cost-effective, and easier to implement in practical systems than active methods [7, 8]. Common examples are twisted tape inserts, helical loops, converging or diverging passages, surface roughness, baffles, gaps, and curved tubes. Among these, corrugated tubes have received significant attention, as their wavy surface geometry can promote boundary-layer disruption, secondary flow generation, and enhanced fluid mixing, all of which contribute to improved convective thermal transfer efficiency [8, 9, 10].

The corrugated tube is characterized by regular geometric graduations on its inner and outer surfaces. Its performance is strongly affected by parameters such as the corrugation amplitude, pitch, and width. By disrupting the flow structure near the wall, corrugations may induce recirculation zones, increase local turbulence, and enhance interaction between the core flow and the wall. These effects usually result in increased heat transfer rates but are often accompanied by increased pressure drop and increased pumping power demand [10, 11, 12]. Therefore, the design of corrugated pipes must balance thermal enhancement against hydraulic drawback.

Despite extensive research on corrugated pipes for convective heat transfer enhancement, most previous publications concentrated mainly on the impacts of geometric parameters and Reynolds numbers on conventional hydrothermal performance indicators, such as the Nusselt number and friction coefficient, without explaining the underlying physics of the synergy between speed and temperature gradient. Moreover, there is still no generally accepted parameter that directly quantifies the efficiency of such synergies in improving the convective heat transfer performance of corrugated pipes. Moreover, although multi-objective optimization is used in related studies, it is often done using absolute performance indices that may not fully capture how design variables affect the improvement relative to a smooth reference configuration.

The aim of this research is therefore to:

i. Establish a synergy-thermal coupling index (STC) to assess the effectiveness of the synergy between velocity and temperature gradient in improving convective heat transfer performance.
ii. Apply the field synergy principle and second-law analysis to explain the mechanism of heat transfer enhancement and entropy generation in outwardly corrugated pipes.

iii. Develop predictive correlations and perform multi-objective optimization to identify the best compromise among thermal enhancement, hydraulic drawback, and entropy production.

This research thus documented a broad framework for evaluating the hydrothermal performance of outwardly corrugated pipes in turbulent flow. Moreover, applying the principle of field synergy provides a clearer physical interpretation of the reinforcement mechanism, and the optimization analysis provides practical guidance for designing efficient heat exchangers and cooling ducts.

2.0: Materials and Methods

2.1. *Description of the physical model of the pipe*

This study investigates forced convective heat transfer of distilled water flowing through a curved tube under turbulent flow conditions generated using ANSYS Inc. [13]. The physical model as generated by ANSYS Inc. [13] is illustrated in Figure 1, and the main geometrical parameters are summarized in Table 1. A three-dimensional model was adopted to better represent the curved geometry and to capture the spatial flow patterns induced by the periodic surface gradients. Unlike the simplified axisymmetric design, the 3D model enables detailed resolution of secondary movements, local recirculation zones, and non-uniform interactions between the core flow and the wall. This is important for a precise assessment of the hydrothermal behaviour of the corrugated pipe, particularly heat transfer enhancement, pressure drop variation, synergy between velocity and temperature gradient, and irreversibility production. The tube has a diameter of 0.03 m, an overall length of 0.8 m, and a corrugation width ratio of $\frac{w}{D} = 0.4$.normalized amplitude in the range $0.03 \leq \frac{e}{D} 0.05$, and normalized pitch in the range $0.9 \leq \frac{P}{D} 1.1$. Outward corrugation modifies the flow pattern near the wall by repeatedly disrupting the boundary layer and forming recirculation zones along the pipe wall. This geometry is therefore expected to enhance mixing between the core flow and the wall fluid, thereby improving heat transfer but also increasing flow resistance. The current setup has been chosen to examine this thermal-hydraulic trade-off and to support the analysis of the field synergy principle and entropy formation.

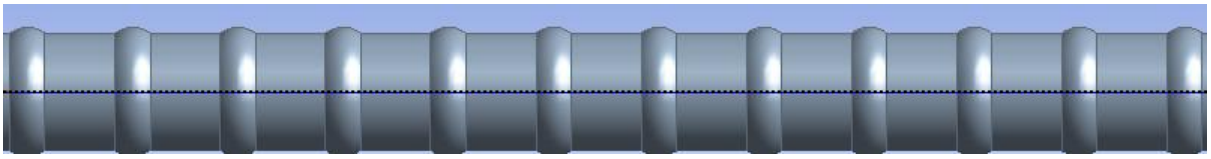


Figure 1: The outwardly Corrugated Pipe (3D geometry)

Table 1: Corrugation parameters

Parameter	Values
Diameter of the pipe(D)	0.03 m
Amplitude of corrugation$\left(\frac{e}{D}\right)$	0.03, 0.04, and 0.05
Pitch of corrugation $\left(\frac{P}{D}\right)$	0.9, 1, 1.1
Width of corrugations $\left(\frac{w}{D}\right)$	0.4
Length of the Pipe (L)	0.8 m

2.2 *Governing Equations*

The turbulent flow of distilled water through the outwardly corrugated pipe was modeled using three-dimensional Reynolds-Averaged Navier-Stokes (RANS) equations, along with the continuum and flow equations. Since the flow is considered non-deterministic and Newtonian, the governing equations are presented in Cartesian tensor form. The SST k-ω turbulence model has been used to close the RANS equations, as it is effective for wall-curved flows with adverse pressure gradients and separation.

$$\frac{\partial}{\partial x_i}\left(\rho_{nf} u_i\right) = 0 \tag{1}$$

$$\frac{\partial}{\partial x_i}\left(u_i u_j\right) = \frac{\partial}{\partial x_j}\left[\mu_f\left(\frac{\partial u_i}{\partial x_j} + \frac{\partial u_j}{\partial x_i} - \frac{2}{3}\delta_{ij}\frac{\partial u_i}{\partial x_j}\right)\right] + \frac{\partial}{\partial x_j}\left(-\rho\overline{\acute{u}_i\acute{u}_j}\right) - \frac{\partial P}{\partial x_i} \tag{2}$$

$$\frac{\partial}{\partial x_i}\left[u_i(\rho E + P)\right] = \frac{\partial}{\partial x_j}\left[\left(k_f + \frac{c_p \mu_t}{Pr_t}\right)\frac{\partial T}{\partial x_j} + u_i \tau_{ij}\right] \tag{3}$$

The RANS was closed using the SST $k-\omega$ model expressed as

$$\frac{\partial}{\partial x_i}(\rho k u_i) = \frac{\partial}{\partial x_j}\left(\Gamma_k \frac{\partial k}{\partial x_j}\right) + \tilde{G}_k - Y_k + S_k \tag{4}$$

$$\frac{\partial}{\partial x_i}(\rho \omega k u_i) = \frac{\partial}{\partial x_j}\left(\Gamma_w \frac{\partial \omega}{\partial x_j}\right) + G_\omega - Y_w + D_\omega + S_\omega \tag{5}$$

Y_k and Y_ω denotes the turbulent dissipations of k and ω,, respectively. More details about $SST\ k-\omega$ is documented in Versteeg and Malalasekera [14].

2.3 *Boundary Conditions*

Inlet : prescribled velocity

Outlet: $P_{gauge} = 0$

Surface: no-slip, $q'' = 10{,}000\ Wm^{-2}$

2.4. *Field synergy principle*

In convective heat transfer systems, the degree of alignment between the velocity vector and the temperature-gradient vector is measured by the field synergy number (FSN). The field synergy principle states that when these two vectors align more closely, the convective transport process improves and heat transfer increases [15, 16].

$$FSN = cos\theta = \frac{\bar{V}.\nabla T}{|V||\nabla T|} \tag{6}$$

The volume average of FSN is obtained by integrating over the test domain

$$\langle FSN \rangle = \frac{\int \bar{V}.\nabla T dV}{\int |V||\nabla T|\, dV} \tag{7}$$

A new term called synergy-thermal coupling (STC) measures the effectiveness of synergy between velocity and temperature gradient in enhancing convective heat transfer performance by estimating the increase in convective heat transfer achieved in a modified pipe compared to a smooth pipe, corresponding to the increase in performance in the modified pipe relative to the smooth pipe.

$$\text{STC} = \frac{Nu^m - 1}{FSN^m - 1} \tag{8}$$

where Nu^m and FSN^m are expressed as

$$Nu^{\,m} = \frac{Nu_{\,mod}}{Nu_{\,stm}}$$

$$FSN^{\,m} = \frac{\langle FSN \rangle_{\,mod}}{\langle FSN \rangle_{\,stm}} \tag{9}$$

where mod and stm represent modified and smooth pipes, respectively

2.5. *Performance indices*

The average Nusselt number (Nu) and friction factor (fr)are expressed as estimated as follows

$$Nu = \frac{hD_h}{k} \tag{10}$$

$$fr = \frac{2D_h \Delta P}{\rho u^2 L} \tag{11}$$

The normalized fr and Nu are expressed as:

$$fr^m = \frac{fr_{mod}}{fr_{stm}} \tag{12}$$

$$Nu^m = \frac{Nu_{mod}}{Nu_{stm}}$$

The performance evaluation criterion (PEC) is expressed as follows:

$$PEC = \frac{Nu^m}{(fr^m)^{1/3}} \tag{13}$$

The volumetric entropy production rate due to temperature and velocity gradients is expressed by Kock and Herwig [17] as follows:

$$S'''_{th} = \frac{1}{\bar{T}^2}\left(k_f + \frac{\mu_{tC_p}}{Pr_t}\right)\left(\frac{\partial \bar{T}}{\partial x_i}\right)^2 \tag{14a}$$

$$S'''_{visc} = \frac{\mu}{\bar{T}}\left(2e_{ij}e_{ij}\right) + \frac{\rho\varepsilon}{T} \tag{14b}$$

The volume average thermal and viscous entropy production rates are expressed as follows:
The total thermal and viscous entropy productions are generated by integrating over the pipe volume [18, 19, 20].

$$\langle S_{th}\rangle = \frac{1}{V}\iiint_{V_0}^{V_1}\left(\frac{1}{\bar{T}^2}\left(k_f + \frac{\mu_{tC_p}}{Pr_t}\right)\left(\frac{\partial \bar{T}}{\partial x_i}\right)^2\right)dV \tag{15a}$$

$$\langle S_{vic}\rangle = \frac{1}{V}\iiint_{V_0}^{V_1}\left(\frac{\mu}{\bar{T}}\left(2e_{ij}e_{ij}\right) + \frac{\rho\varepsilon}{T}\right)dV \tag{15b}$$

The volume average entropy production rate becomes

$$\langle S_{gen}\rangle = \langle S_{th}\rangle + \langle S_{vic}\rangle \tag{16}$$

The normalized irreversibility (S^m) is expressed as

$$S^m = \frac{\langle S_{gen}\rangle_{mod}}{\langle S_{gen}\rangle_{stm}} \tag{17}$$

2.6 *Regression Analysis*

The regression analysis of diamensionaless output variables Y can be written in terms of nondiamensioanles input variables $X_1, X_2, X_3, \ldots X_{n-1}, X_n$ as follows:

$$Y = \alpha X_1^{m1} X_2^{m2} X_3^{m3} \ldots X_{n-1}^{m(n-1)} X_n^{mn} \tag{18}$$

In this study, the inut variables are Re, $\frac{e}{D}$ and $\frac{P}{D}$. Equation (3.35) becomes:

$$Y = \alpha Re^{m1}\left(\frac{e}{D}\right)^{m2}\left(\frac{P}{D}\right)^{m3} \tag{19}$$

We linearize this by applying natural logarithm:

$$\ln(Y) = \ln(\alpha) + m1\ln(Re) + m2\ln\left(\frac{e}{D}\right) + \mathrm{m3}\ln\left(\frac{P}{D}\right) \tag{20}$$

We can estimate $\ln(\alpha)$, $m1$, $m2$ and $m3$ from the obtained data by writing simple programs in MATLAB

2.7 Multi-objective optimization

This work aims to maximize Nu^G and minimize $\langle S_{gen} \rangle^G$ and fRe^G subject to the following constraints: $0.03 \leq \frac{e}{D} \leq 0.05, 0.9 \leq \frac{P}{D} \leq 1.1$ & $5.0 \times 10^3 \leq Re \leq 4.0 \times .10^4$. This is achieved using the non-dominated sorting algorithm (NSG-II) in order to determine the optimum solution (Pareto front).

3.0 Results and Discussion

This section presents and discusses the results of the CHTP and EPR simulations of distilled H_2O flow through an outwardly corrugated pipe. It focuses on the influence of the amplitude of corrugation $\left(0.03 \leq \frac{e}{D} \leq 0.05\right)$, pitch of corrugation $\left(0.9 \leq \frac{P}{D} \leq 1.1\right)$ and flow conditions $(5.0 \times 10^3 \leq Re \leq 4.0 \times 10^4)$ on $Fc, Nu, fr, PEC, and \langle S_{gen} \rangle$. The first subsection presents the contours of the field variables; the second subsection focuses on the parametric study; and the last section focuses on multi-objective optimization

3.1 *Grid sensitivity test and validation*

The grid dependence test was conducted on corrugated pipes of $\frac{e}{D} = 0.05$ and $\frac{p}{D} = 1.1$ at $Re = 4.0 \times 10^4$. This was achieved by varying the number of grids employed in the calculation. The variation in the number of grids against the estimated values of Nu is shown in Table 2. The error between the 1093617 and 1288525 mesh configurations for Nu is 0.06%; therefore, the 1288525 mesh configuration was used for the remaining simulations. For validation purposes, we considered the work of Sun and Zeng [21], where the authors carried out an experimental investigation that measured the Nu of dry air flowing in corrugated pipes with the following corrugation parameters ($\frac{e}{D} = 0.088$, $\frac{P}{D} = 1.1$) spanning the range of $1.0 \times 10^4 \leq Re \leq 4.0 \times 10^4$. The same problem was simulated, and the results obtained were compared with the experimental values; both agreed to a great extent. The average percentage error was less than 5%, as shown in Figure 2. Furthermore, we investigated the hydrothermal performance of water in straight pipes under fully developed flow conditions and compared the results obtained by Nu and fr with the existing correlation developed by Dittus and Boelter [22] for Nu and Blasius [23] for fr. Comparisons of the two correlations with the present results are shown in Figure 3 and Figure 5, respectively. The two comparisons strongly agreed with the existing correlations, and the average errors attributed to Nu were 4.01% and the corresponding value for fr was 5.04%. Finally, we estimate the entropy production rate in straight pipes under fully developed flow conditions and compare the results obtained with the analytical solution developed by [24]. A comparison of the two results is shown in Figure 2. The two results closely matched, with an average error of less than 6.93%. These results demonstrate that our model is accurate for investigating hydrothermal performance and the entropy production rate in this study.

Table 2: Grid Indepedence Test

Number of mesh	Nu	Deviation(%)
392238	293.1755032	
602028	300.7927254	2.532382468
677803	303.5228739	0.899486889
982289	305.86	0.764116304
1093617	306.0509	0.06237525
1288525	306.2419192	2.532382468

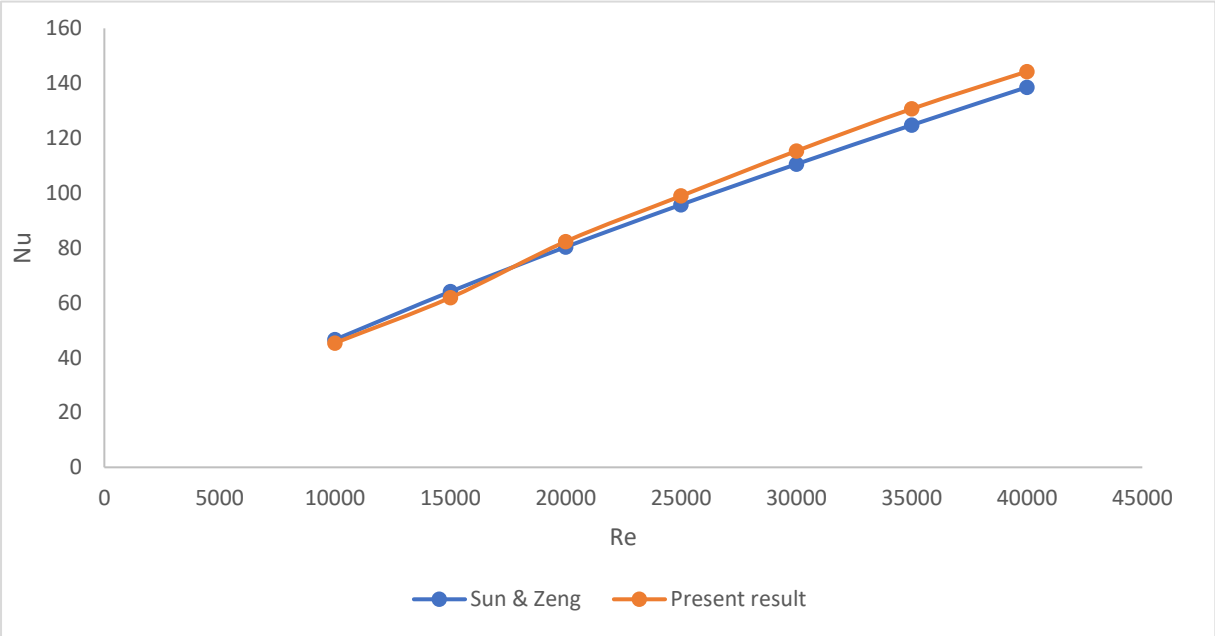


Figure 2: Validation of the experimental results of Sun and Zeng [21]

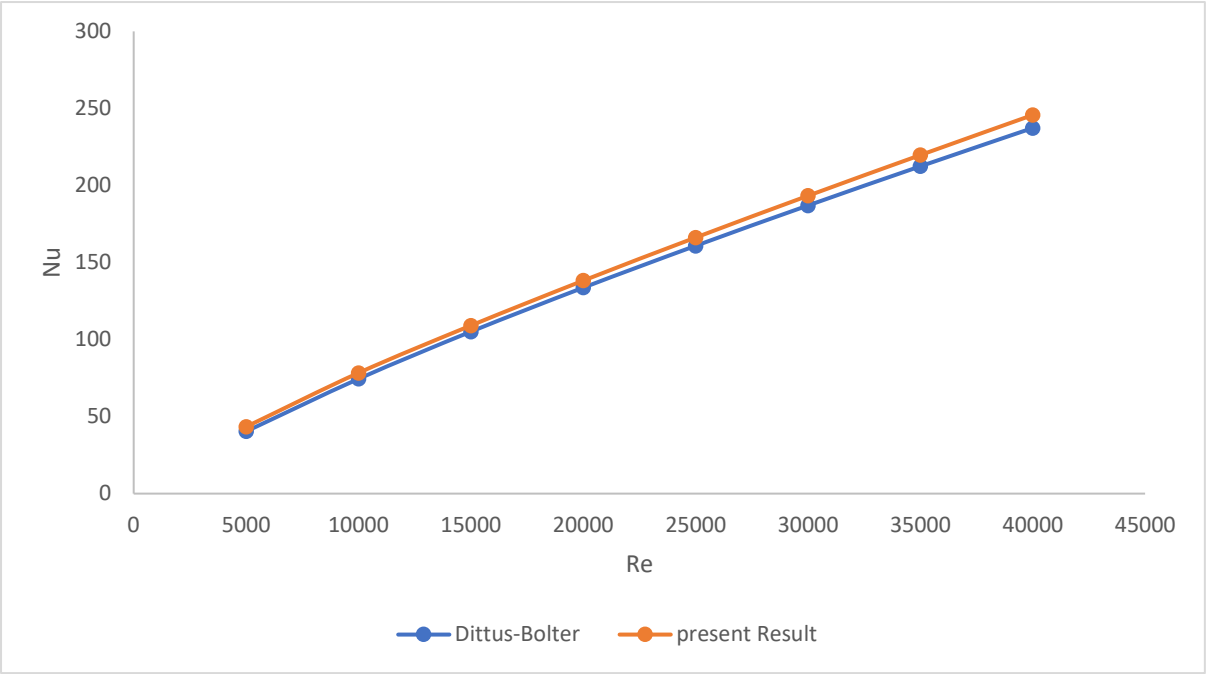


Figure 3: Validation of Nu with Dittus & Boelter [22] correlation

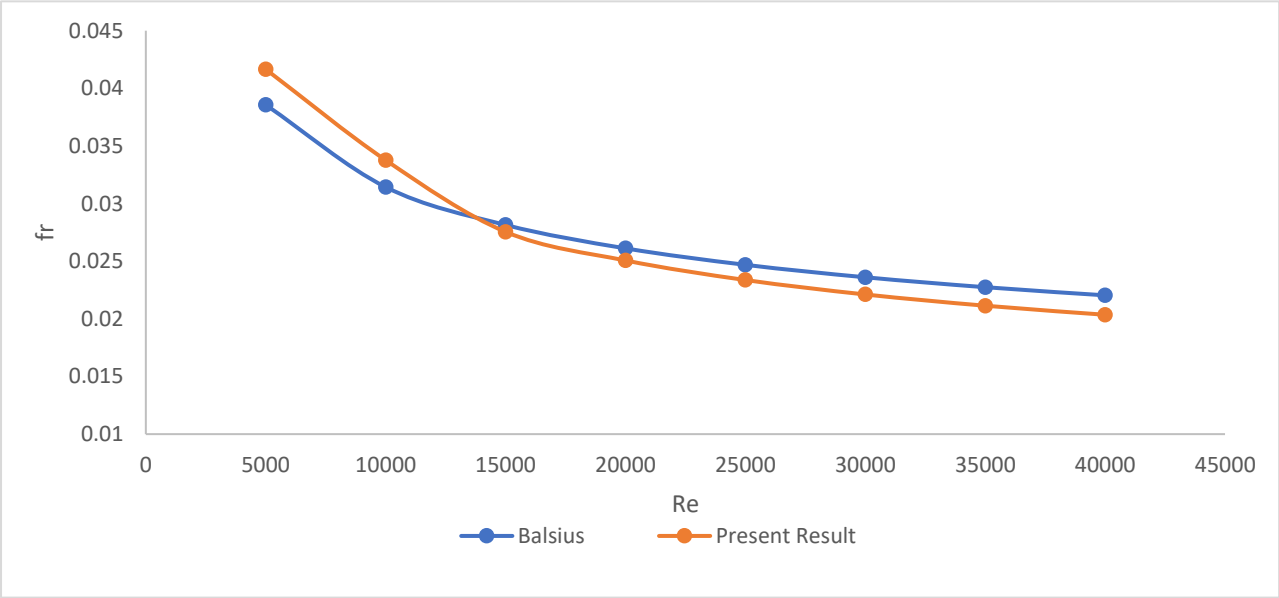


Figure 4: Validation of fr with the correlation of Blasius [23]

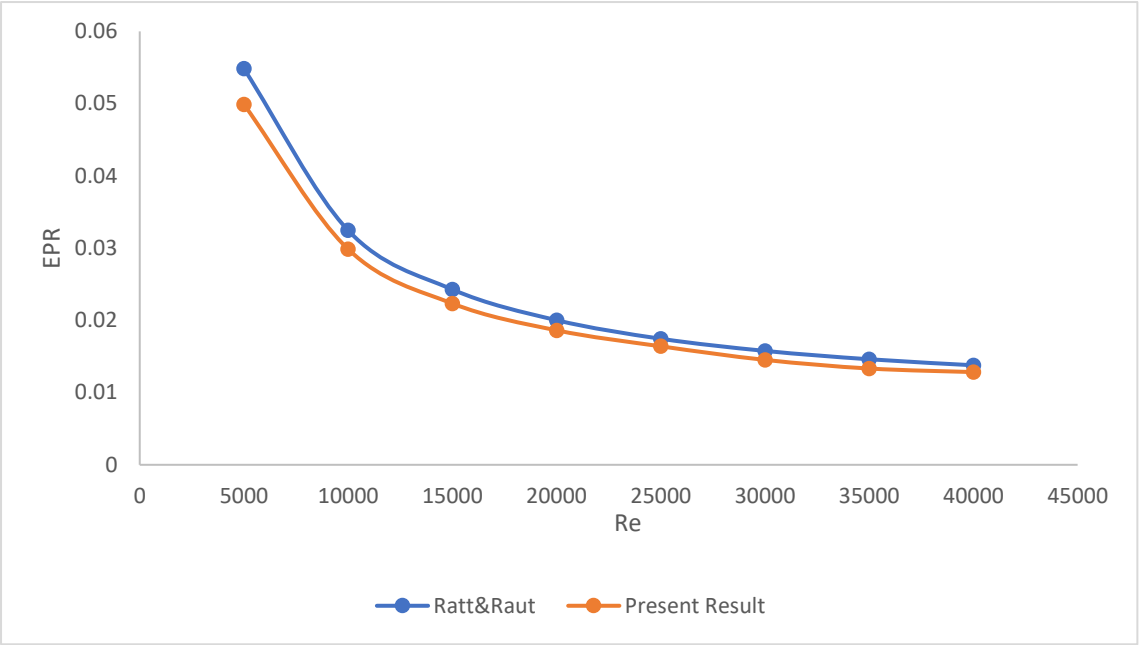
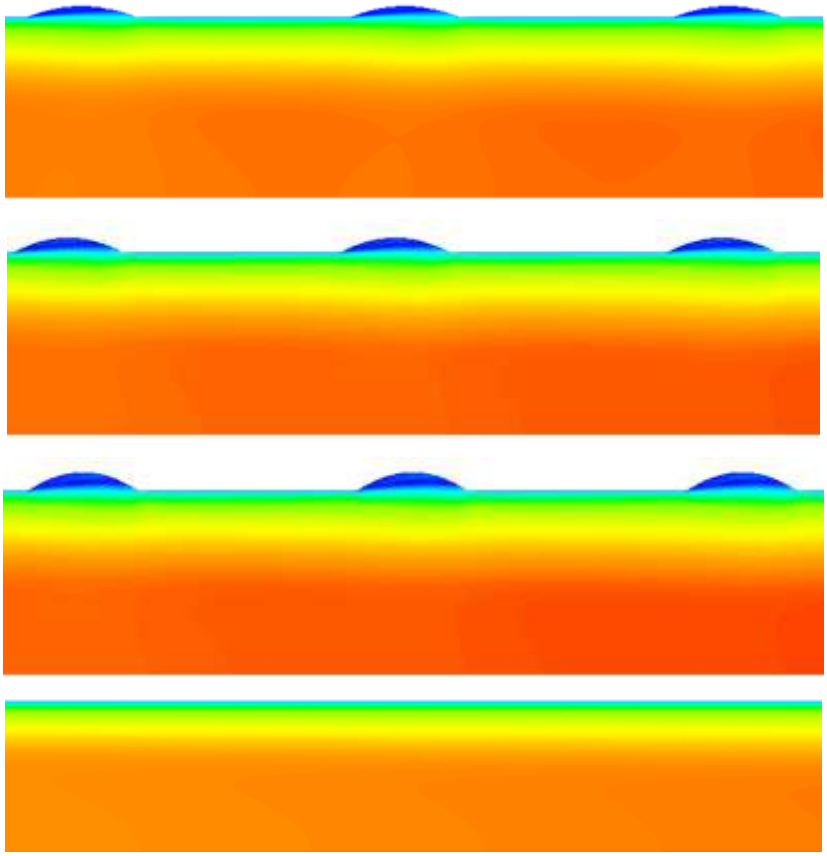


Figure 5: Validation of S_{gen} with the analytical solution of Ratt and Raut [24].

3.2 *Contours*

Figure (6-10) provides the contour plots of velocity, pressure, turbulent kinetic energy, temperature, field synergy number, and entropy generation, respectively, provide a clear physical picture of how corrugation alters the internal flow structure. In the following discussion, a smooth pipe serves as a reference case, and the effect of corrugation amplitude is highlighted by comparing it with the modified geometry. Velocity contours show zero velocity at the wall and maximum velocity at the pipe's center, which is expected. In corrugated tubes, the flow is often disturbed by curved walls, leading to local separation and recirculation zones. As the amplitude increases, these recirculation areas become more pronounced and cover a larger part of the flow domain, resulting in stronger mixing between the fluid near the walls and the core fluid. This increased mixing plays a key role in the improved convective heat transfer observed in the modified pipeline. Pressure contours show that the curved tubes experience a larger pressure drop than the flat tubes. This is because the repeated expansion and contraction of the flow passage, caused by the corrugation geometry, increases flow resistance and produces negative pressure gradients at the peaks and troughs of the corrugations. As the amplitude rises, the pressure variation becomes more noticeable, confirming that the hydraulic pressure grows with greater corrugation amplitude. The turbulent kinetic energy contours show that the corrugated tubes produce more turbulence than the smooth tubes, especially in the near-wall region where velocity gradients are greatest. As a result, turbulent kinetic energy is concentrated around the corrugation zones and increases with increasing corrugation amplitude. This trend confirms that outward corrugations promote turbulence, increasing momentum exchange and improving thermal mixing. The temperature contours indicate a smoother thermal field in smooth tubes, whereas corrugated tubes display a noticeable thermal disturbance caused by boundary layer disruption. In modified pipes, the temperature distribution is

less uniform near the corrugated wall, as vortical structures repeatedly transfer heat from the wall to the main flow. As the corrugation amplitude increases, the thermal boundary layer (TBL) becomes thinner and more permeable, enhancing heat transfer from the wall to the liquid. The field synergy number (FSN) contours also demonstrate the effect of corrugation on the alignment between the velocity and temperature gradient. Less synergy is observed in smooth tubes, where the velocity and temperature gradient fields mostly remain orthogonal. In corrugated tubes, the development of radial velocity components improves local alignment in certain areas, especially around corrugated peaks, leading to higher FSN values. However, in recirculation zones, low FSN regions still occur where flow direction opposes the temperature gradient. Overall, the intensity of the FSN increases with greater corrugation amplitude, indicating improved transport through synergy. The entropy production contours show that thermal entropy generation (S'''_{th}) is concentrated near the wall, where the temperature gradient is strongest, while viscous entropy generation (S'''_{vic}) is also concentrated there due to the high velocity gradients in the boundary layer. In corrugated tubes, both entropy generation fields are strongly distorted by surface profiles. This suggests that, although corrugation increases heat transfer, it also alters the distribution of irreversibility in the flow field. Furthermore, we noticed a zone near the surface of the corrugation where S'''_{vic} has minimum values and the size increases with increasing $\frac{e}{D}$. This is attributed to the increase in the recirculation zone as $\frac{e}{D}$ increases. Notably, the recirculation zone is characterized by a low-velocity gradient.



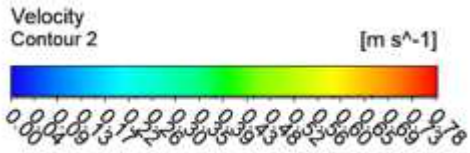
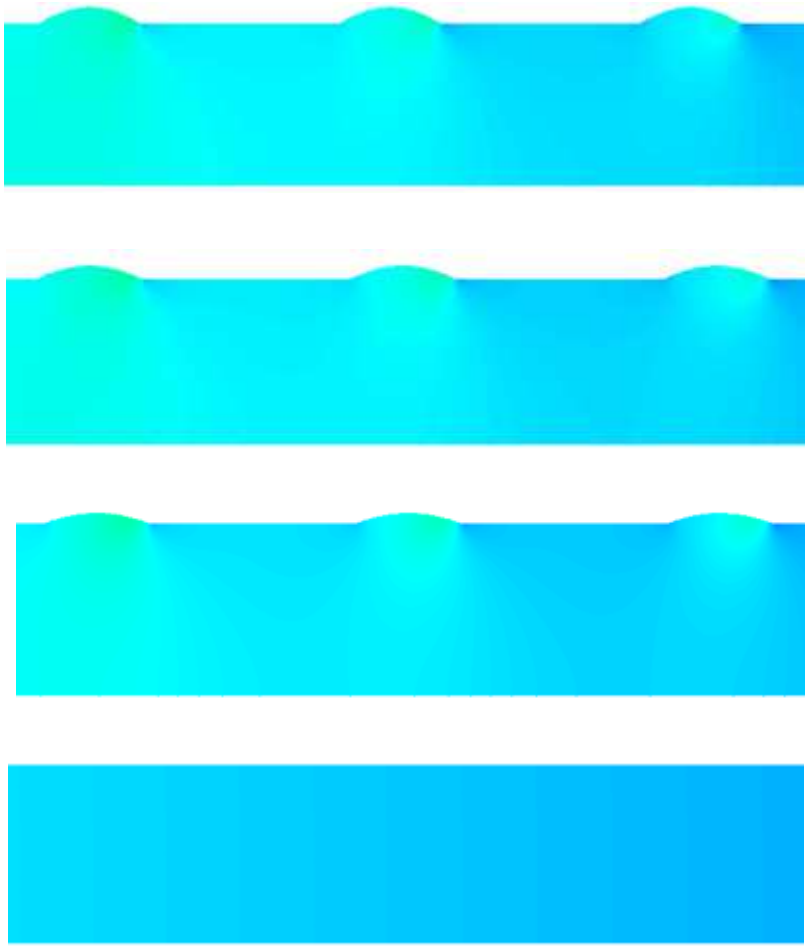


Figure 6: Contours of velocity in the staright and corrugated pipes for various $\frac{e}{D}$ values



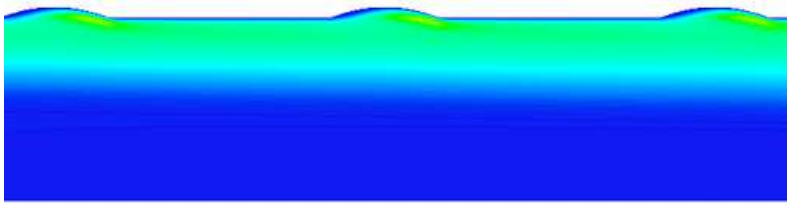
$\frac{e}{D} = 0.05$

$\frac{e}{D} = 0.04$

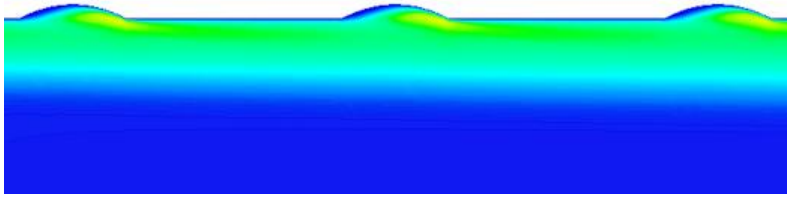
$\frac{e}{D} = 0.03$

Straight

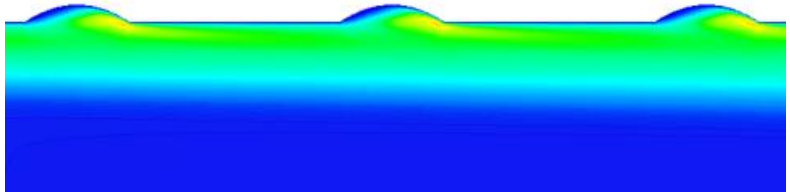
Figure 7: Contours of pressure in the staright and corrugated pipes for various $\frac{e}{D}$ values



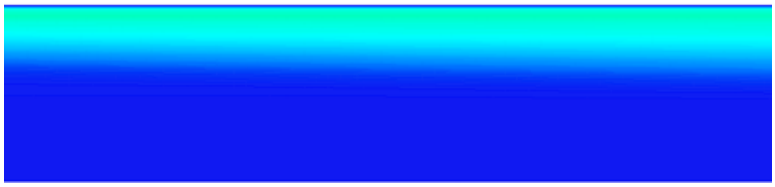
$\frac{e}{D} = 0.03$



$\frac{e}{D} = 0.04$



$\frac{e}{D} = 0.05$



Straight

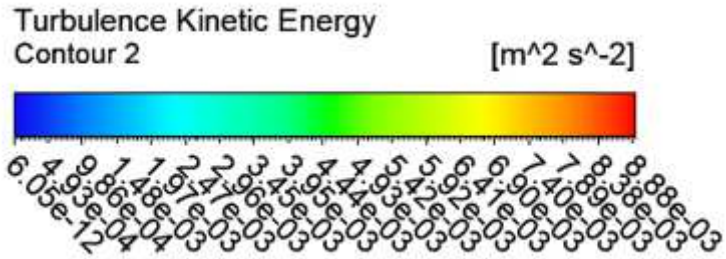
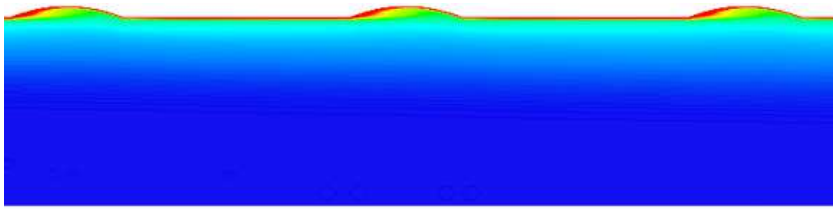
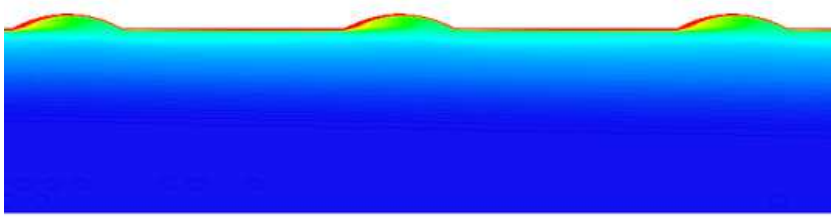


Figure 8: Contours of TKE in the staright and corrugated pipes for various $\frac{e}{D}$ values



$\frac{e}{D} = 0.03$



$\frac{e}{D} = 0.04$

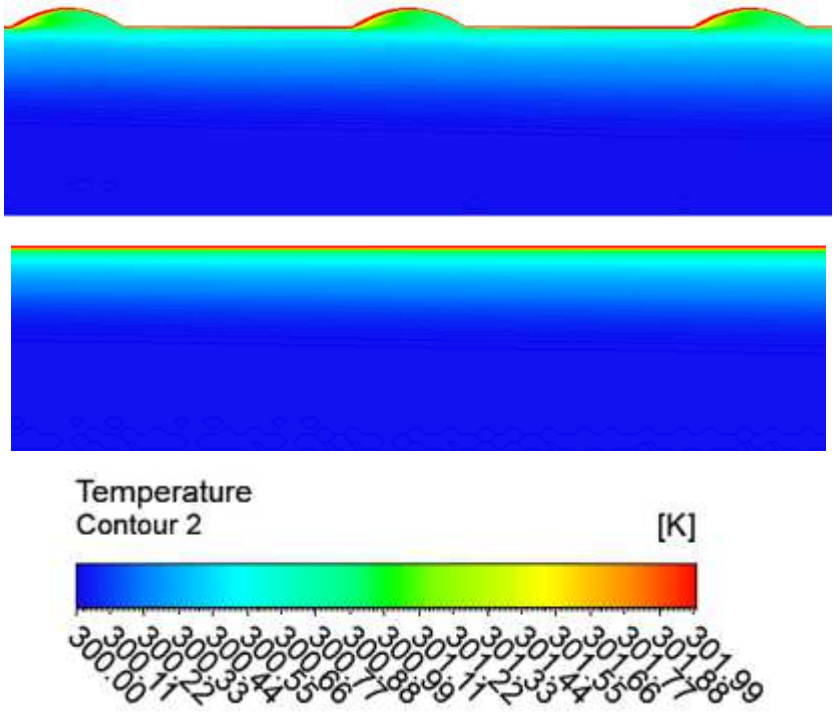
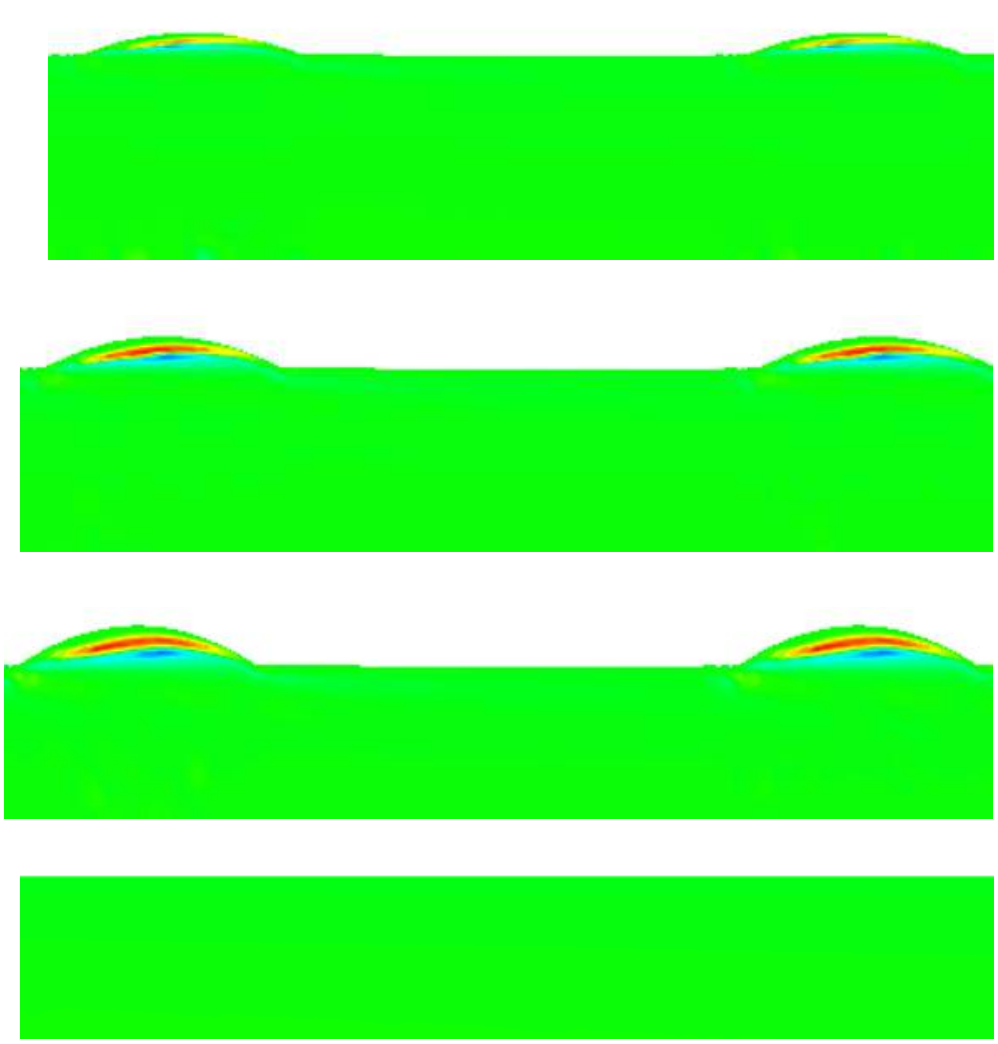


Figure 9: Contours of the temperature in the staright and corrugated pipes for various $\frac{e}{D}$ values



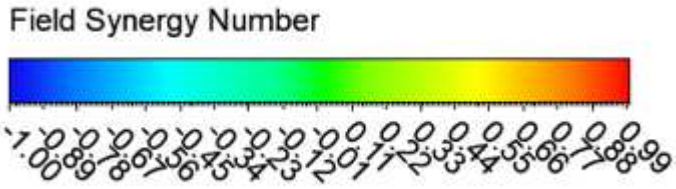


Figure 10: Contours of the FSN in the staright and corrugated pipes for various $\frac{e}{D}$ values

3.3 Parametric studies

3.3.1: Field Synergy Number

Figure 11 and Figure 12 described the change in the average FSN with Reynolds number for smooth tubes and corrugated tubes with different $\frac{e}{D}$ at constant $\frac{P}{D}$, respectively. In all cases, the corrugated tubes exhibit a higher FSN than the smooth tubes, indicating better alignment between the velocity and temperature gradient fields in the modified geometry. This improvement is more pronounced as the $\frac{e}{D}$ increases. At $Re = 2.0 \times 10^4$,, the FSN in corrugated pipe with $\frac{e}{D} = 0.03$ is 0.076, and the corresponding value in the straight pipe is 0.06. This increase can be linked to the radial component of corrugation, which improves the interaction between the flow field and the thermal field. Consequently, the convective transport process is more efficient in a corrugated configuration. As Reynolds numbers increase, FSN decreases for both smooth and curved tubes. The reduction factors over the whole Reynolds number range are 0.91, 0.88, and 0.82 for $\frac{e}{D} = 0.03, 0.04$ & 0.05, respectively. This trend indicates that greater turbulence at higher Reynolds numbers increases recirculation and non-uniform flow patterns, reducing the degree of effective alignment between velocity and temperature gradients. The effect of the corrugation's amplitude is also apparent in the results. FSN values increase from 0.078 to 0.088 as $\frac{e}{D}$ rises from 0.03 to 0.05. This confirms that larger corrugation amplitudes increase the synergy between the flow and heat (thermal) fields by enhancing radial transport. Increasing the $\frac{p}{D}$, on the other hand, has a slightly opposite effect. At $Re = 1.5 \times 10^4$, the values of FSN in corrugated pipes with $\frac{e}{D} = 0.03$ and $\frac{P}{D}$ $0.9, 1.0$ and 1.1 are 0.082, 0.08, and 0.077, respectively. This indicates that larger pitch values slightly reduce FSN, as the number of corrugating elements along the flow path decreases, thereby reducing the frequency of interference and the intensity of the radial mixing process. Overall, the results show that the corrugation amplitude has a higher impact on the field synergy number than the straight pipe.

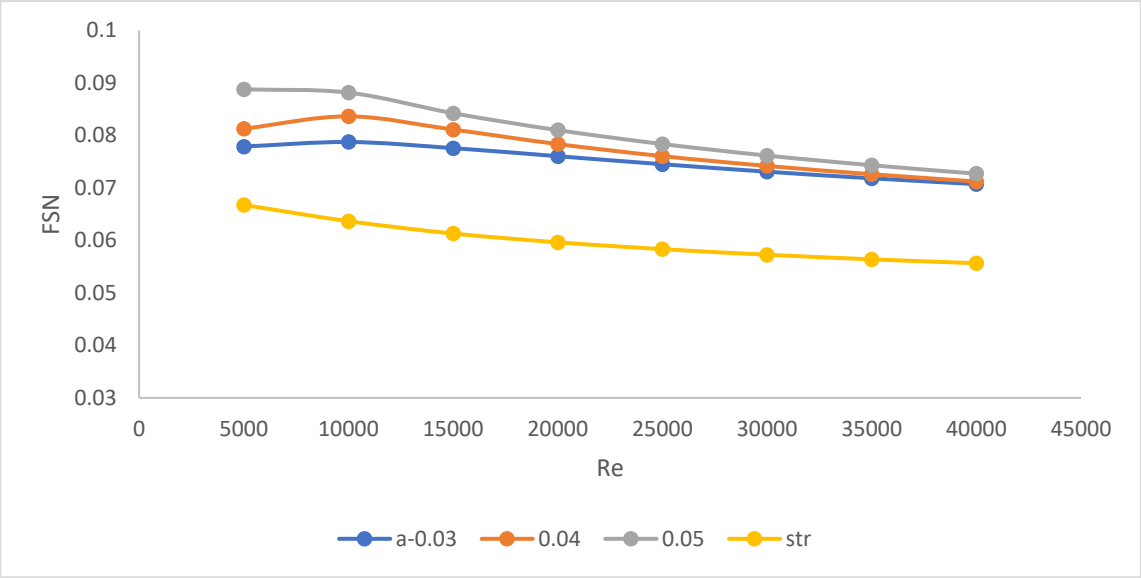


Figure 11: Variation in FSN against Re for various values of $\frac{e}{D}$

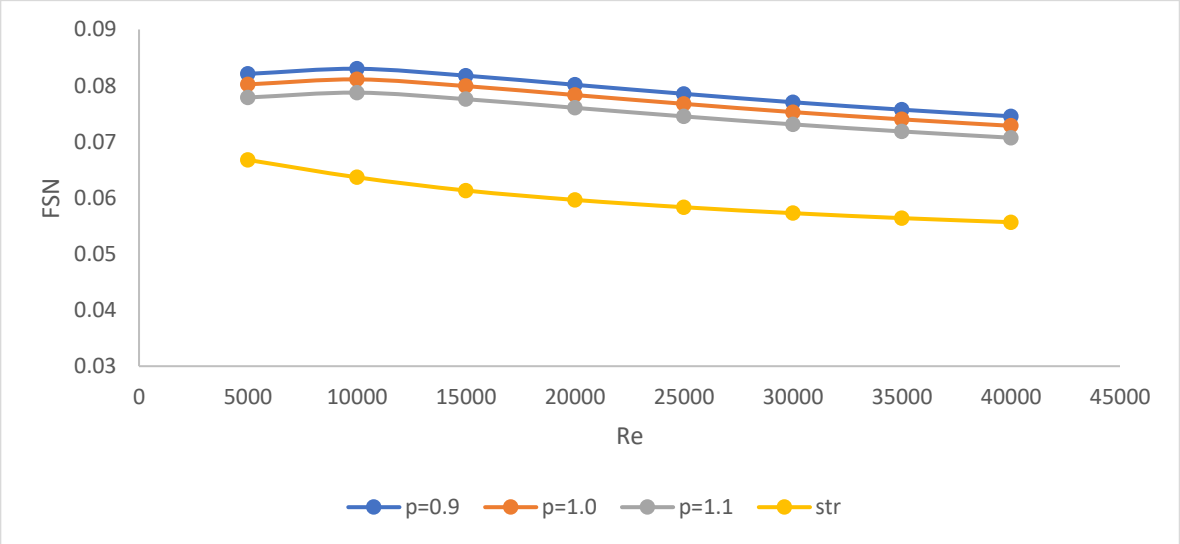


Figure 12: Variation in FSN against Re for various values of $\frac{P}{D}$

3.3.2 Friction factor

Figure 13 shows the variation of the friction coefficient with Reynolds number for smooth and curved pipes of various $\frac{e}{D}$ values while $\frac{P}{D}$ remain constant. In all cases, the corrugated tubes exhibit a higher friction coefficient than the smooth tubes, confirming that the corrugated geometry induces greater flow resistance. This behavior is expected because a curved wall continuously distorts flow and increases the wall shear stress. For example at $Re = 2.0 \times 10^4$, the coefficient of friction for the corrugated tube of $\frac{e}{D} = 0.03$ is 0.028, as opposed to 0.025 for the straight tube. The higher friction factor is due to repeated flow separation and reconnection caused by the corrugations, leading to increased momentum loss and pressure drop. As the

amplitude of the corrugation increases, so does the friction coefficient at $Re = 1.0 \times 10^4$, the values of fr in the corrugated pipes of $\frac{e}{D} = 0.03, 0.04\ and\ 0.05$ are 0.033, 0.035, and 0.037, respectively. This trend indicates that a stronger corrugation amplitude enhances turbulence and intensifies recirculation flow. The effect of the pitch is somewhat less pronounced but is nevertheless perceptible at $Re = 1.5 \times 10^4$, the values of fr in corrugated pipes with $\frac{e}{D} = 0.03$ and $\frac{P}{D}$ $0.9, 1.0\ and\ 1.1$ are 0.031, 0.03, and 0.029, respectively. The slight decrease in fr with increasing pitch is attributed to fewer corrugation elements per unit strip length, which reduces the frequency of disturbances to the flow and thus the resistance. Overall, the results indicate that increasing the Reynolds number decreases the coefficient of friction, whereas increasing the corrugation amplitude increases it. The corrugated tube, therefore, offers better heat transfer at the cost of a higher pressure drop as depicted in Figure 14, and the final design must balance these competing effects.

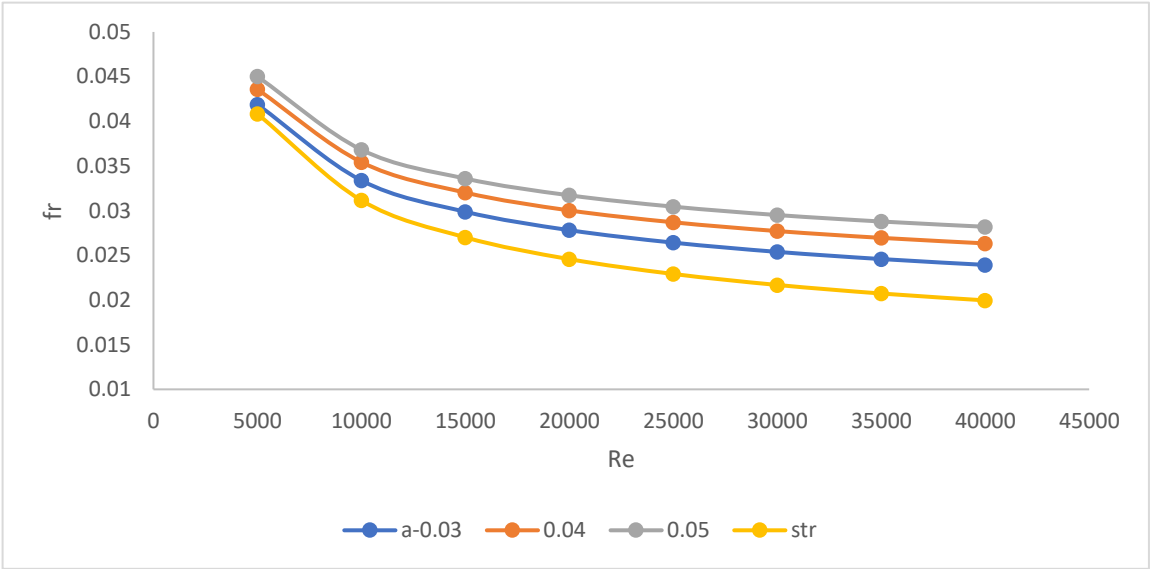


Figure 13: Variation in fr against Re for various values of $\frac{e}{D}$

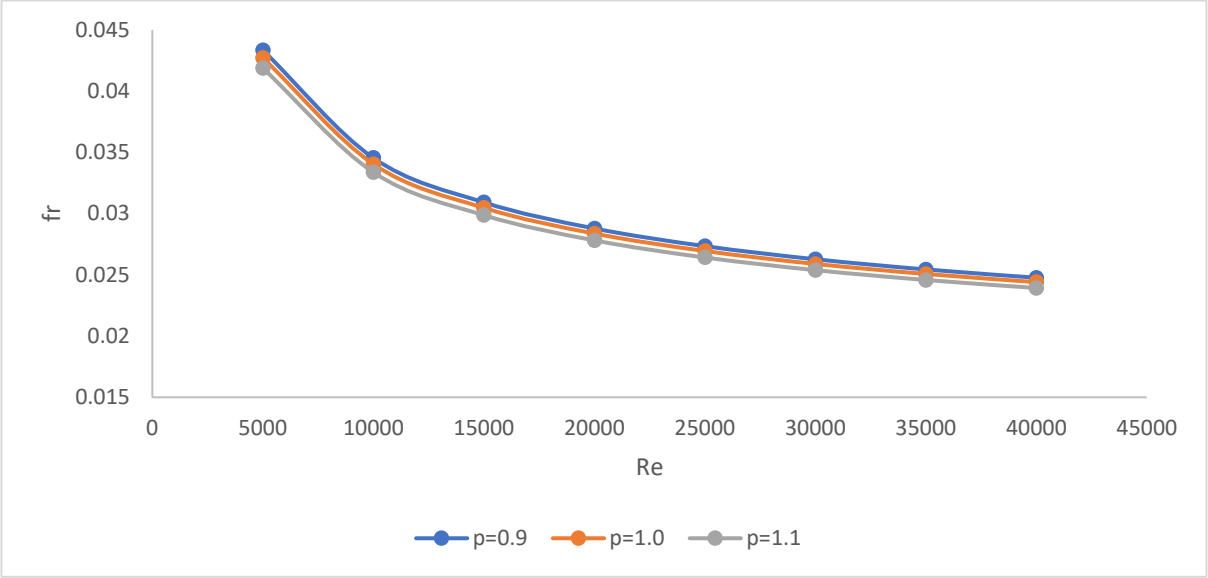


Figure 14: Variation in fr against Re for various values of $\frac{P}{D}$

3.3.3 Nusselt number

Figure 15 and Figure 16 illustrates the variation of the Nu with Reynolds number for both the smooth pipe and the corrugated pipes across different values of e/D and P/D. In all instances, the corrugated pipes demonstrate higher Nu than the smooth pipe, thereby confirming that the corrugated geometry augments convective heat transfer. This phenomenon is attributed to the combined effects of boundary layer disruption, increased turbulence generation, and enhanced field synergy, all of which contribute to improved heat transfer from the wall to the fluid core. As Reynolds number increases, the Nu also increases for both the smooth and corrugated pipes. Over the entire range of Reynolds numbers considered, the Nu increases by factors of 5.98, 5.19, and 4.81 for the corrugated pipes of $e/D =$ 0.03, 0.04 & 0.05, respectively, while the smooth pipe increases by a factor of 5.54. This trend is expected because higher Reynolds numbers promote stronger turbulent mixing, thinner thermal boundary layers, and faster transport of thermal energy away from the wall. The effect of e/D is also clearly visible. At $Re = 1.0 \times 10^4$, the values of $Nu$for $e/D = 0.03$, 0.04, and 0.05 are 91.77, 100.43, and 105.49, respectively. The increase in amplitude strengthens the flow disturbances and enhances the radial motion, leading to more effective mixing and a higher rate of heat transfer. In contrast, increasing the $\frac{P}{D}$ produces a slight reduction in the Nu. At $Re = 1.5 \times 10^4$, the values of Nu for $e/D =$ 0.03and $P/D = 0.9$, 1.0, and 1.1 are 131.72, 130.75, and 129.03, respectively. This behavior is attributed to the reduced number of corrugation elements along the pipe length at higher pitch values, which weakens the frequency of boundary-layer disturbance and slightly lowers the heat transfer enhancement. Overall, the findings indicate that corrugation amplitude exerts a more substantial influence than pitch. Furthermore, higher Reynolds numbers and increased corrugation amplitudes both contribute to enhanced convective heat transfer. These observations align with the phenomena of augmented turbulence generation, the thinning of the TBL and the intensified field synergy induced by the outwardly corrugated geometry.

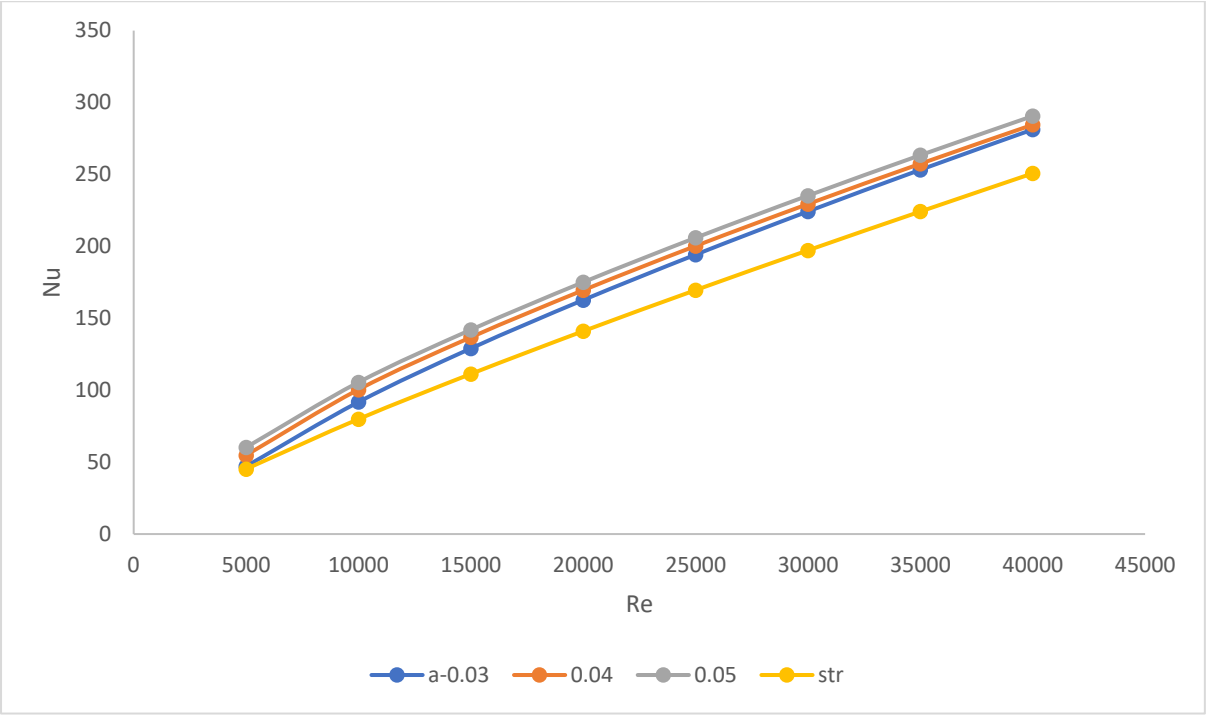


Figure 15: Variation in Nu against Re for various values of $\frac{e}{D}$

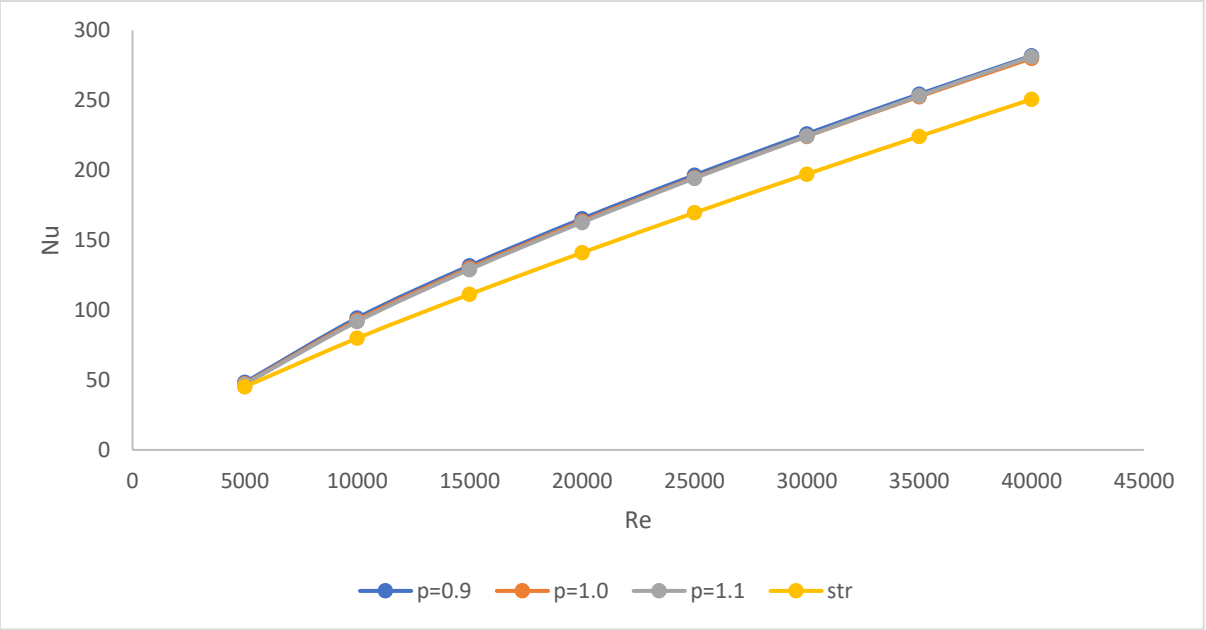


Figure 16: Variation in Nu against Re for various values of $\frac{P}{D}$

3.3.4 Performance evaluation criterion

Figure 17 illustrates the different performance evaluation criterion (PEC) with Reynolds number for corrugated pipes at different corrugation amplitudes and pitch. The PEC offers a convenient way to assess the thermal-hydraulic trade-off by comparing the increase in heat transfer with the associated rise in frictional

losses. Values above unity indicate that the thermal advantages of the modified pipe outweigh its hydraulic drawbacks compared to the smooth pipe. For all the corrugated configurations evaluated, the PEC remained above unity across the entire Reynolds number range, confirming that the outwardly corrugated pipe offers better overall performance than the smooth pipe. At low Reynolds numbers, the increase in heat transfer is significant enough to offset the rise in pressure drop, especially at larger corrugation amplitudes. $Re = 5.0 \times 10^3$, the values of PEC in the corrugated pipes of $\frac{e}{D} = 0.03, 0.04\ and\ 0.05$ are 1.03, 1.18, and 1.29, respectively. The corresponding values at $Re = 4.0 \times 10^5$ are 1.06, 1.04, and 1.03, respectively. As the Reynolds number increases, the PEC decreases for the higher-amplitude corrugations. Throughout the entire range of Reynolds numbers, the PEC decreases by factors of 0.08 and 0.87 of $\frac{e}{D} = 0.04\ and\ 0.05$ respectively, while for of $\frac{e}{D} = 0.03$ The PEC slightly increased by a factor of 1.02. The influence of pitch is relatively weaker than that of amplitude. The plots for different pitch ratios show only minor variation. This indicates that corrugation amplitude is the primary geometric parameter controlling PEC in the current setup, while pitch plays a secondary role. Overall, the results show that the optimal thermal-hydraulic balance is found at relatively low Reynolds numbers and moderate corrugation levels, where heat transfer improvement stays significantly larger than the pressure-drop drawback.

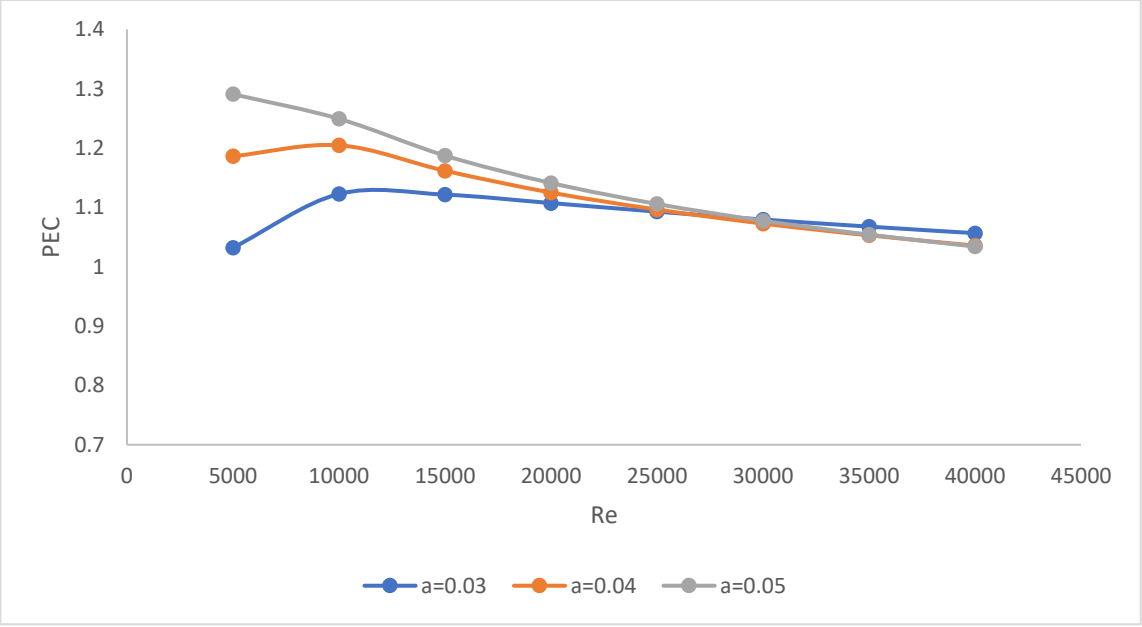


Figure 17: Variation in PEC against Re for various values of $\frac{e}{D}$

3.3.5 Synergy-thermal coupling

The STCI identifies three different operating regimes: STCI > 1 indicates a synergy-amplified regime where improvements in field synergy are efficiently converted into Nu enhancement, with wall-normal transport being highly effective and minimal energy diverted into unproductive recirculation; STCI = 1 represents a balanced synergy boundary where thermal increase is exactly proportional to the increase in synergy; and

STCI < 1 indicates a synergy-limited regime where part of the increased synergy results from vortex circulation and turbulent kinetic energy generation, which increase the area-averaged thermal energy efficiency without proportionally contributing to thermal transfer, thus producing a decreasing thermal return. The results showed that when D = 0.04, the system reaches STCI ≈ 1.00 at Re = 5,000, exactly at the equilibrium synergy threshold, which is the optimal value for converting synergy into Nu at low Re, with a non-monotonic profile that rises to approximately 0.62 at Re = 5,000. The maximum, about 0.62, occurs at Re = 10,000, reflecting the geometric activation limit below which the shallow gradient is not sufficiently energized to channel the products of synergy effectively into heat transfer to the walls. All amplitude cases operate within the synergy-limited regime with STCI < 1 at high Re. For pitch variation, all cases remain entirely below STCI = 1 across all conditions, indicating negligible sensitivity in low-to-moderate Re regimes above 20,000. The case with p = 1.1 maintains the highest STCI, which is attributed to the greater axial separation between the corrugation elements, providing an additional linear distance for the interaction between production reattachment and the TBL at low Re. This confirms that amplitude primarily controls the activation of synergy at low Re, while pitch governs the sustained conversion efficiency at high Re through different physical mechanisms.

3.3.6. Thermal entropy generation rate

Figure (18) illustrates the variation of ⟨S‴_th⟩ with Re for the straight pipe and corrugated pipes with various $\frac{e}{D}$ and $\frac{P}{D}$. The results show that corrugated pipes exhibit a lower $\langle S_{th} \rangle$ than the straight pipe across the range of Re considered. For instance, at $Re = 2.0 \times 10^4$, the value of $\langle S_{th} \rangle$ for the corrugated pipe with e/D = 0.03 is 43.01 $Wm^{-3}K^{-1}$, compared with 49.60 $Wm^{-3}K^{-1}$ for the straight pipe. This is expected because corrugation decreases the thermal boundary-layer thickness and enhances turbulence production, which reduces the temperature gradient and, consequently, $\langle S_{th} \rangle$ In addition, an increase in Re reduced $\langle S_{th} \rangle$ for all pipe geometries. For instance across the range of Re ($(5.0 \times 10^3 \leq Re \leq 4.0 \times 10^4)$, considered $\langle S_{th} \rangle$ in corrugated pipes with $\frac{e}{D}$ = 0.03, 0.04, and 0.05 decreased to approximately 0.17, 0.20, and 0.21 of their respective initial values, compared with a corresponding reduction factor of 0.18 for the straight pipe. This outcome is expected because higher turbulence intensity progressively thins the thermal boundary layer with increasing Re, thereby lowering $\langle S_{th} \rangle$ Furthermore, increasing$\frac{e}{D}$ decreased $\langle S_{th} \rangle$. For example, at Re = 1.0 × 10^4, the outcomes of ⟨S‴_th⟩ for corrugated pipes with $\frac{e}{D}$ = 0.03, 0.04, and 0.05 are 75.70, 69.17, and 65.87 $Wm^{-3}K^{-1}$, respectively. This result is expected because increasing corrugation amplitude enhances turbulence, which reduces the temperature gradient and thereby decreases $\langle S_{th} \rangle$. In contrast, increasing P/D led to a marginal increase in $\langle S_{th} \rangle$ For instance, at Re = 1.5 × 10^4, the values of $\langle S_{th} \rangle$ for corrugated pipes with $\frac{e}{D}$ = 0.03 and P/D = 0.9, 1.0, and 1.1 are 51.39, 52.48, and 54.10 $Wm^{-3}K^{-1}$, respectively as depicted in Figure 19.

This is expected because increasing $\frac{P}{D}$ causes less distortion of the thermal boundary layer and reduces turbulence, thereby increasing $\langle S_{th} \rangle$.

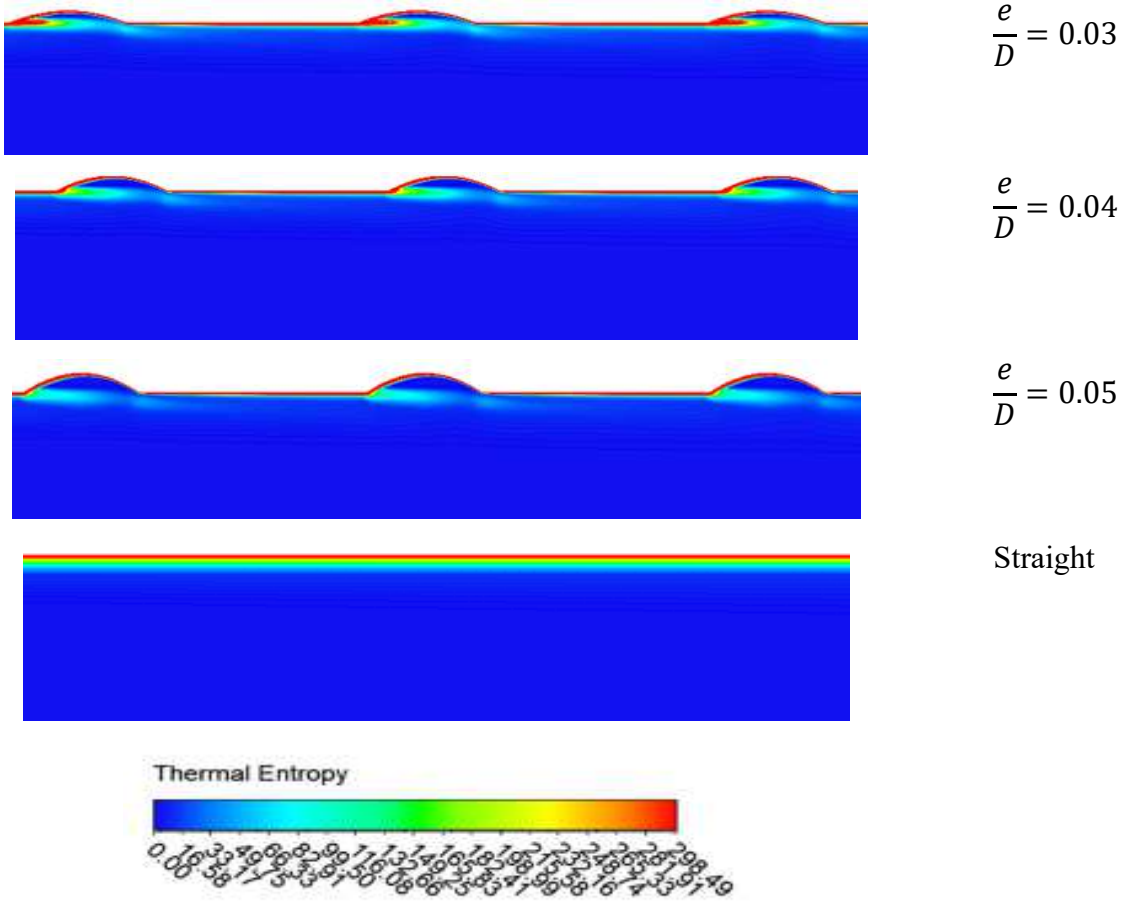


Figure 18: Contours of S_{th}''' in the staright and corrugated pipes with various $\frac{e}{D}$ values

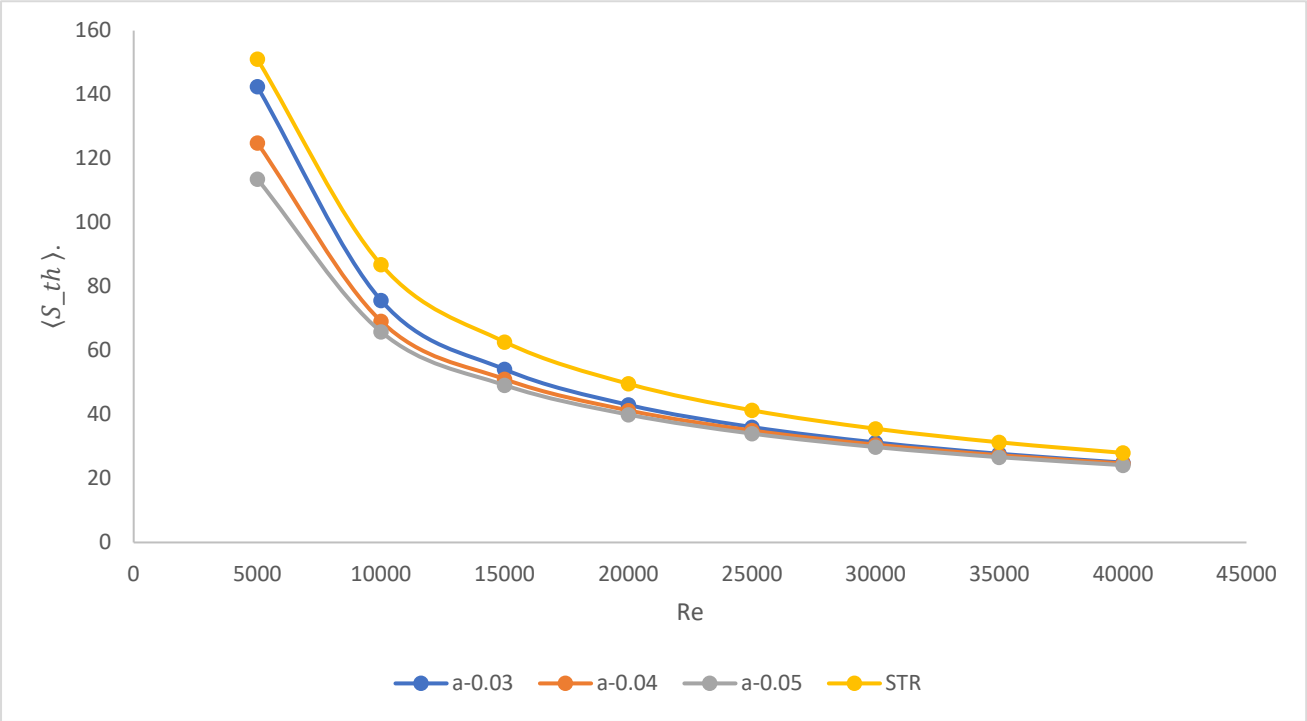


Figure 19: Variation in $\langle S_{th} \rangle$ against Re for various values of $\frac{e}{D}$

3.3.7. Viscous enytropy production rate

Figure (20) shows how $\langle S_{vic} \rangle$ varies with Re for the straight pipe and corrugated pipes with various $\frac{e}{D}$ and $\frac{P}{D}$. The results demonstrate that corrugated pipes exhibit higher $\langle S_{vic} \rangle$ than the straight pipe. For instance, at Re = 2.0×10^4, the corrugated pipe with $\frac{e}{D}$ = 0.03 has $\langle S_{vic} \rangle$ = 3.14 $Wm^{-3}K^{-1}$, compared with 2.67 $Wm^{-3}K^{-1}$ for the straight pipe. This result is expected because corrugations enhance the velocity gradient and the eddy dissipation rate (ε), thereby increasing $\langle S_{vic} \rangle$. In addition, a rise in Re increased $\langle S_{vic} \rangle$ for all pipe geometries. For instance, across the range of Re considered, $\langle \langle S_{vic} \rangle$ in the corrugated pipes of $\frac{e}{D}$ = 0.03, 0.04, and 0.05 increased by factors of approximately 37.02, 39.17, and 40.60, respectively, compared to a corresponding increase factor of 31.18 for the straight pipe. This result is expected, as an increase in Re enhances the velocity gradient and eddy dissipation rate throughout the domain. Furthermore, an increase in $\frac{e}{D}$ increased $\langle S_{vic} \rangle$ For instance, at Re = 1.0×10^4, the values of $\langle S_{vic} \rangle$ for the corrugated pipes of e/D = 0.03, 0.04, and 0.05 are 0.94, 0.99, and 1.03 $Wm^{-3}K^{-1}$, respectively. This result is expected, as an increase in corrugation amplitude enhances turbulence, which strengthens the velocity gradient and eddy dissipation, leading to an increase in $\langle S_{vic} \rangle$ In contrast, an increase in $\frac{P}{D}$ led to a marginal decrease in $\langle S_{vic} \rangle$ For instance, at Re = 1.5×10^4, the values of $\langle S_{vic} \rangle$ for the corrugated pipes with $\frac{e}{D}$ = 0.03 and P/D = 0.9, 1.0, and 1.1 are 2.26, 2.21, and 2.13 $Wm^{-3}K^{-1}$, respectively as depicted in Figure 21 and Figure 22. This is expected as an increase in $\frac{P}{D}$ leads to reduced turbulence production, consequently decreasing $\langle S_{vic} \rangle$. Notably, for brevity, the variation in ⟨S‴_gen⟩

against Re is not presented, as the trend closely resembles that of $\langle S_{vic} \rangle$. This is because $\langle S_{vic} \rangle$ dominates $\langle S_{vic} \rangle$ throughout the range of Re, geometric amplitude, and pitch considered.

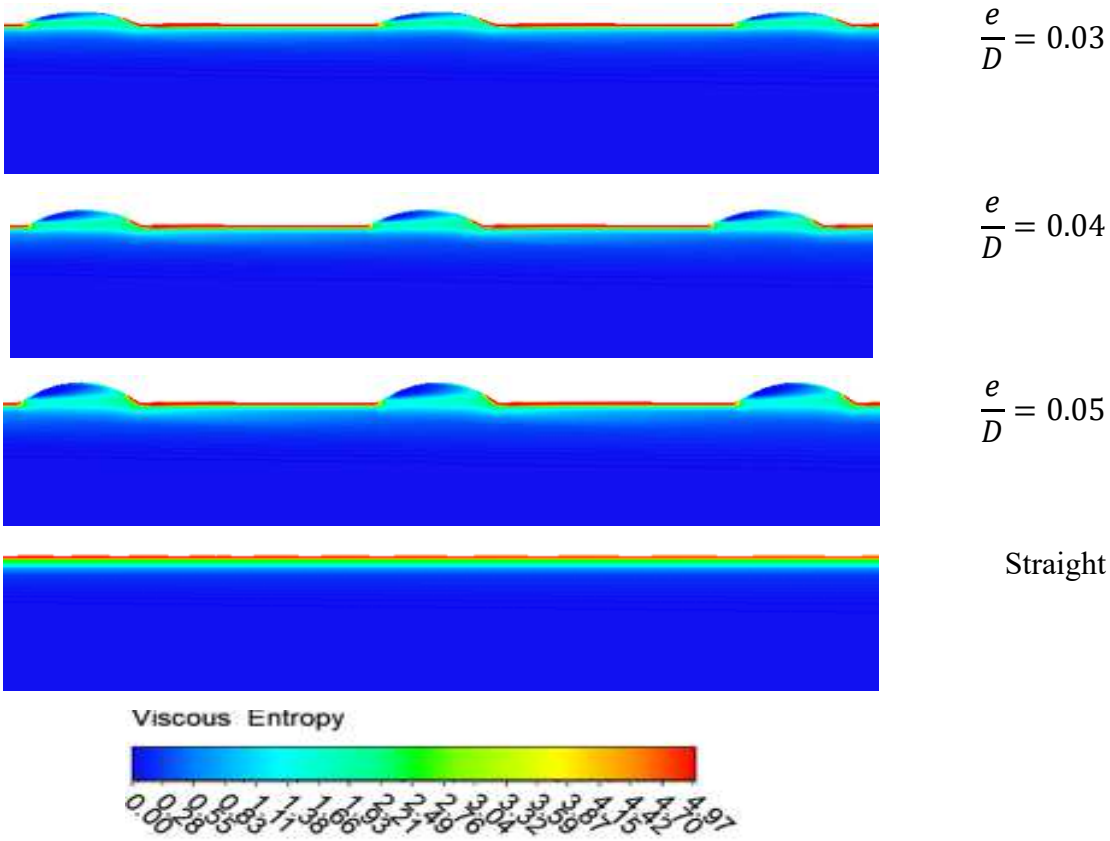


Figure 20: Contours of S'''_{vic} in the staright and corrugated pipes with various $\frac{e}{D}$ values

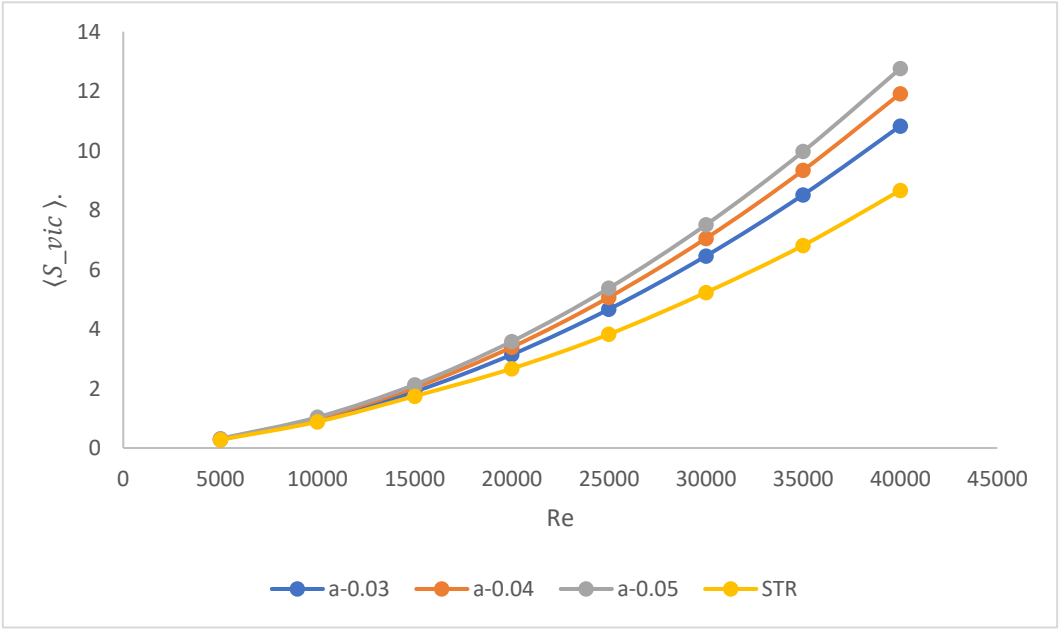


Figure 21: Variation in $\langle S_{vic} \rangle$ against Re for various values of $\frac{e}{D}$

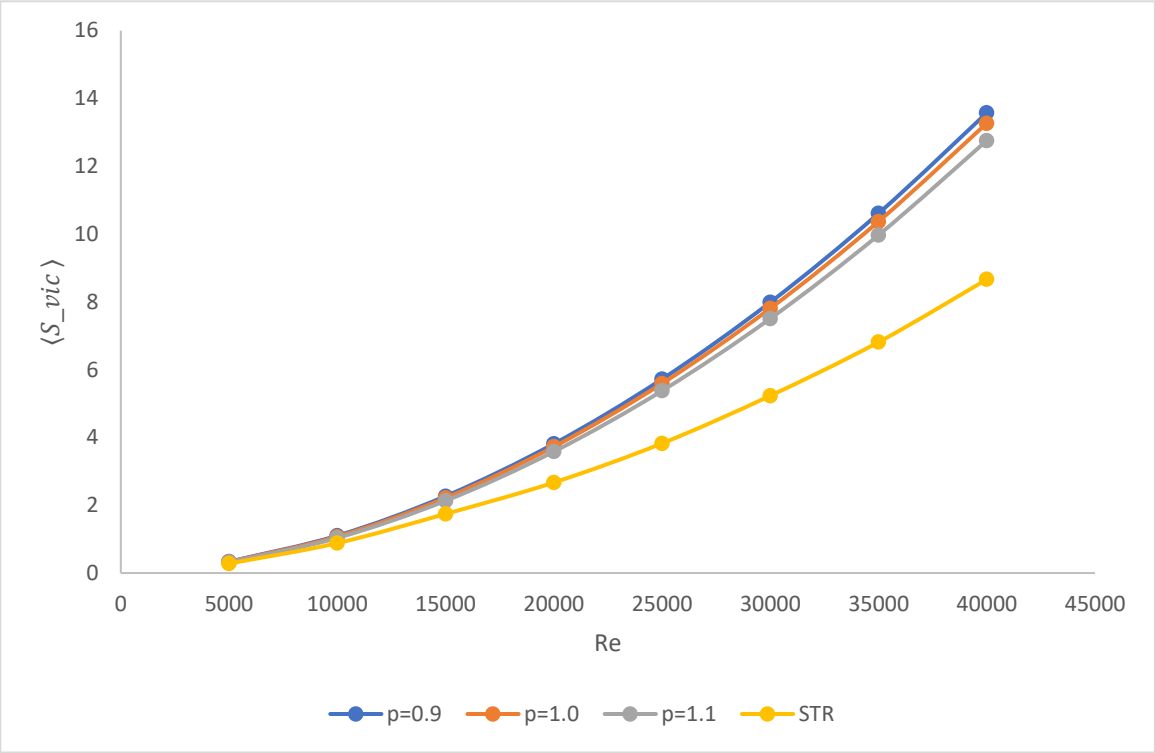


Figure 22: Variation in $\langle S_{vic} \rangle$ against Re for various values of $\frac{P}{D}$

3.4.1 Regression Analysis

The results of the regression analysis for Nu^G, fRe^G and $\langle S_{gen} \rangle^G$ as a function of the input variables Re, $\frac{P}{D}$ and $\frac{e}{D}$ are depicted in Table 3. The R^2 outcomes for Nu^G, fRe^G and $\langle S_{gen} \rangle^G$ are 0.873, 0.917 and 0.895, respectively. This implies that the regression models gave accurate predictions about variations in Nu^G, fRe^G and $\langle S_{gen} \rangle^G$ as a result of the three independent variables (Re, $\frac{P}{D}$ and $\frac{e}{D}$). In addition, for Nu^G, the exponents of Re and $\frac{P}{D}$ are nagetive, whereas that of $\frac{e}{D}$ is positive. This is expected as efficeincy of passive techniaue in enahncing convective heat tarnsfer perfromance decreases as Re and $\frac{P}{D}$ increases. Regarding fRe^G. The exponent of Re and $\frac{e}{D}$ are postive while that of $\frac{P}{D}$ is negative. This is also expected as increase in Re and $\frac{e}{D}$ enahnces pressure drop by increasing the turbulence production while increase in $\frac{p}{D}$ decrease the turbulence production. Consequently reduction in pressure drop. Lastly for $\langle S_{gen} \rangle^G$ both Re and $\frac{P}{D}$ have postive exponent while $\frac{e}{D}$ has negative exponent.

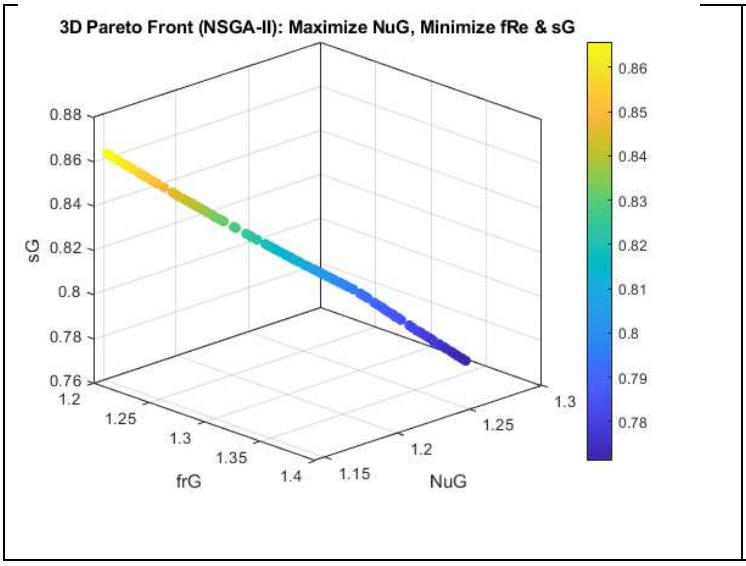
Table 3. Result of regression Analysis

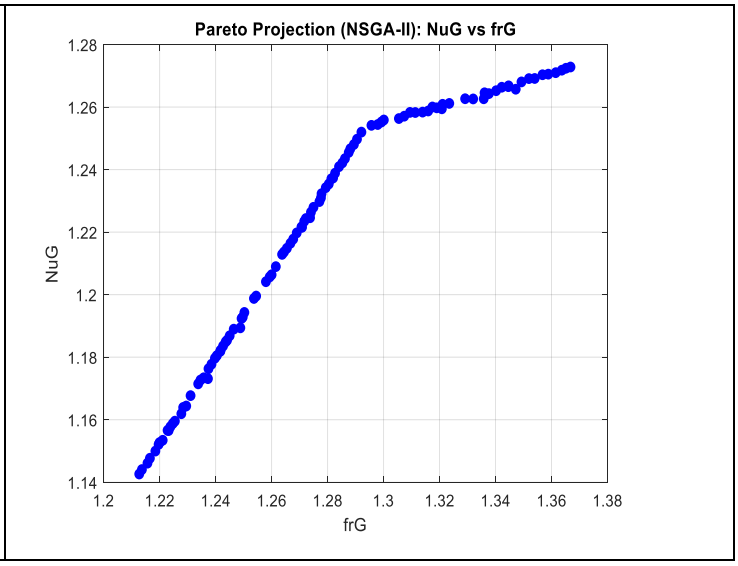
Regression	R^2

$Nu^G = 2.37Re^{-0.0097}\left(\frac{e}{D}\right)^{0.1825}\left(\frac{p}{D}\right)^{-0.0729}$	0.873
$fRe^G = 1.58Re^{0.0242}\left(\frac{e}{D}\right)^{0.1269}\left(\frac{p}{D}\right)^{-0.2760}$	0.917
$\langle S_{gen}\rangle^G = 0.444Re^{0.0065}\left(\frac{e}{D}\right)^{-0.1708}\left(\frac{p}{D}\right)^{0.1427}$	0.895

3.4.2 Pareto front

The result of multi-object optimization (pareto front) is described in Figure (23). The results showed that the NSGA-II algorithm successfully produced a well-converged Pareto front for the corrugated pipe optimization. All Pareto-optimal solutions achieved $Nu^G > 1$, fRe^G in the range 1.21–1.37, and $\langle S_{gen}\rangle^G$ in the range 0.77–0.87, confirming that the CP outperforms the STR in both thermal and thermodynamic performance despite the attendant hydraulic drawback. The $Nu^G - fRe^G$ projection showed a concave trade-off profile with diminishing returns beyond $Nu^G \approx 1.25$, implying an increasing marginal hydraulic cost per unit of thermal augmentation at higher corrugation intensities. The $Nu^G - \langle S_{gen}\rangle^G$ projection showed a monotonically graph, establishing that enhanced CHTP is accompanied by a net reduction in irreversibility, as the corrugation-driven suppression of TEPR outweighs the concurrent rise in viscous VEPR. Furthermore, the $\langle S_{gen}\rangle^G - fRe^G$ projection confirmed that higher-friction configurations correspond to lower EPR, consistent with corrugation-induced recirculation flow promoting thermal mixing more effectively than it elevates viscous dissipation. Consequently, solutions in the range $Nu^G \approx 1.20$–1.25 represent the optimal design compromise for hydraulically-constrained applications.





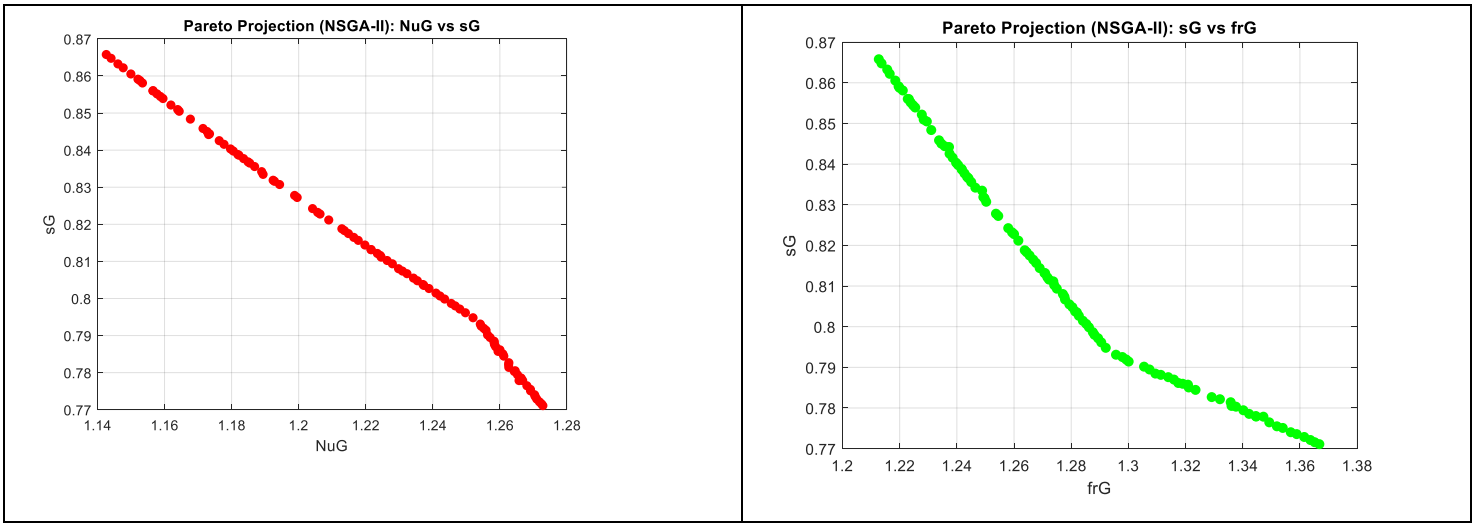


Figure 23: Pareto front for the multi-objective optimization

4. Conclusions

In this research, a comprehensive investigation of the turbulent hydrothermal performance of distilled water flowing through outwardly corrugated pipes from the perspective of the first and second thermodynamic laws was performed focusing, on the influence of flow conditions $(5.0 \times 10^3 \leq \leq 4.0 \times 10^3)$ and corrugation parameters, such as the normalized amplitude $\left(0.03 \leq \frac{e}{D} \leq 0.05\right)$ and normalized pitch $\left(0.9 \leq \frac{p}{D} \leq 1.1\right)$, on selected hydrothermal performance indices, such as the average Nusselt number (Nu), friction factor (fr), performance evaluation criterion (PEC), average volumetric entropy production rate for $(\langle S_{gen} \rangle)$ and field synergy number. The main findings include but are not limited to the following:

1. Increase in Re and $\frac{e}{D}$ enhances both CHTP and hydraulic pressure drop. However, the opposite is the case for $\frac{P}{D}$. in addition, FSN decrease with increasing Re and $\frac{P}{D}$.

2. The results of STC revealed that the enhancement of CHTP observed cannot be entirely attributed to synergy between velocity and temperature gradient.

3. The result of the regression showed that $\frac{e}{D}$ has positive index to thermal enhancement while Re and $\frac{P}{D}$ have negative indices. However, both Re and $\frac{e}{D}$ have positive indices for hydraulic enhancement.

4. The $Nu^G - fRe^G$ projection of the Pareto front showed a concave trade-off profile with diminishing returns beyond $Nu^G \approx 1.25$, implying an increasing marginal hydraulic cost per unit of thermal augmentation at higher corrugation intensities

5. Within the range of Re considered TEPR dominate VEPR this cause decrease in EPR as Re and $\frac{e}{D}$ increase.

Declarations

Consent for publication

The submission of this research was accepted and approved by the author.

Conflicting interests

Competing interests

There are no conflicts of interest for the authors.

Funding Declaration

No funding.

Reference

[1] M. W. Azam, U. Sajjad, F. Maqbool, and G. Sempirini, "Enhancing Heat Exchanger Performance through Passive Techniques: A Comprehensive Review," *Frontiers in Heat and Mass Transfer*, vol. 24, no. 1, pp. 1–10, 2026, doi: 10.32604/fhmt.2025.074690.

[2] C. Yu, M. Shao, W. Zhang, M. Huang, and G. Wang, "Enhancing heat transfer efficiency in corrugated tube heat exchangers: A comprehensive approach through structural optimization and field synergy analysis," *Heliyon*, vol. 10, no. 9, p. e30113, May 2024, doi: 10.1016/j.heliyon.2024.e30113.

[3] M. E. Haque, M. S. Hossain, and H. M. Ali, "Laminar forced convection heat transfer of nanofluids inside non-circular ducts: A review," *Powder Technology*, vol. 378, pp. 808–830, Jan. 2021, doi: 10.1016/j.powtec.2020.10.042.

[4] W. Liao and S. Lian, "Effect of compound corrugation on heat transfer performance of corrugated tube," *International Journal of Thermal Sciences*, vol. 185, p. 108036, Mar. 2023, doi: 10.1016/j.ijthermalsci.2022.108036.

[5] A. A. Owojori, B. A. Olokuntoye, and O. G. Fadodun, "Numerical investigation of second law analysis of PGGNP/H2O nanofluid in various converging pipes," *International Nano Letters*, vol. 11, no. 1, pp. 43–57, Jan. 2021, doi: 10.1007/s40089-020-00321-x.

[6] C. S. Iweka and O. G. Fadodun, "Numerical modeling of heat transfer in Al2O3/H2O nanofluid flowing through a Bessel-like converging pipe," *Archives of Thermodynamics*, pp. 121–153, July 2021, doi: 10.24425/ather.2021.137557.

[7] S. A. Kadhim *et al.*, "Enhancing the thermal performance of double-pipe heat exchangers using wire coil inserts: A focused review," *Scientific African*, vol. 29, p. e02896, Sept. 2025, doi: 10.1016/j.sciaf.2025.e02896.

[8] G. Musielak, D. Mierzwa, and J. Łechtańska, “Experimental Investigation of Enhancement of Natural Convective Heat Transfer in Air Using Ultrasound,” *Applied Sciences*, vol. 13, no. 4, p. 2516, Feb. 2023, doi: 10.3390/app13042516.

[9] M. V. Bidari, P. B. Nagaraj, K. Rajesh, G. Lalagi, and J. K. Panda, “Numerical and experimental analysis of laminar flow heat transfer in a circular tube using metallic inserts,” *Heat and Mass Transfer*, vol. 62, no. 7, July 2026, doi: 10.1007/s00231-026-03725-1.

[10] Y. S. Chen, J. Tian, Y. Fu, Z. F. Tang, H. H. Zhu, and N. X. Wang, “Experimental study of heat transfer enhancement for molten salt with transversely grooved tube heat exchanger in laminar-transition-turbulent regimes,” *Applied Thermal Engineering*, vol. 132, pp. 95–101, Mar. 2018, doi: 10.1016/j.applthermaleng.2017.12.054.

[11] S. O. Oke, P. Gao, O. G. Fadodun, and A. Kaood, “Numerical investigation on hydrothermal characteristics and entropy generation rate of novel composite corrugated pipes in the intermediate heat exchanger of a supercritical CO2 direct cycle gas fast reactors,” *Nuclear Engineering and Design*, vol. 446, p. 114562, Jan. 2026, doi: 10.1016/j.nucengdes.2025.114562.

[12] O. G. Fadodun, O. O. Fadodun, and A. Kaood, “Hydrothermal performance and entropy production rate in distilled H2O flowing in a converging corrugated pipe with increasing corrugation parameters,” *International Communications in Heat and Mass Transfer*, vol. 172, p. 110457, Mar. 2026, doi: 10.1016/j.icheatmasstransfer.2025.110457.

[13] ANSYS Inc. (2022). *ANSYS Fluent theory guide*.

[14] H. Versteeg and W. Malalasekra, *An introduction to computational fluid dynamics*. Prentice Hall, 2007.

[15] J. Guo, M. Xu, and L. Cheng, “The application of field synergy number in shell-and-tube heat exchanger optimization design,” *Applied Energy*, vol. 86, no. 10, pp. 2079–2087, Oct. 2009, doi: 10.1016/j.apenergy.2009.01.013.

[16] Z. Y. Guo, W. Q. Tao, and R. K. Shah, “The field synergy (coordination) principle and its applications in enhancing single phase convective heat transfer,” *International Journal of Heat and*

Mass Transfer, vol. 48, no. 9, pp. 1797–1807, Apr. 2005, doi: 10.1016/j.ijheatmasstransfer.2004.11.007.

[17] F. Kock and H. Herwig, "Local entropy production in turbulent shear flows: a high-Reynolds number model with wall functions," *International Journal of Heat and Mass Transfer*, vol. 47, no. 10–11, pp. 2205–2215, May 2004, doi: 10.1016/j.ijheatmasstransfer.2003.11.025.

[18] S. Majid and J. Mohammad, "Optimal selection of annulus radius ratio to enhance heat transfer with minimum entropy generation in developing laminar forced convection of water-Al2O3 nanofluid flow," *Journal of Central South University*, vol. 24, no. 8, pp. 1850–1865, Aug. 2017, doi: 10.1007/s11771-017-3593-7.

[19] Y. Ji, H.-C. Zhang, X. Yang, and L. Shi, "Entropy Generation Analysis and Performance Evaluation of Turbulent Forced Convective Heat Transfer to Nanofluids," *Entropy*, vol. 19, no. 3, p. 108, Mar. 2017, doi: 10.3390/e19030108.

[20] D. Zhang, H. Zhang, Q. Wang, and W. Sun, "Effect of Heat Flux Distribution on Entropy Generation and Irreversibility of Lead-Bismuth Eutectic (LBE) Forced Convective Heat Transfer," *Journal of Thermal Science*, vol. 32, no. 1, pp. 223–236, Dec. 2022, doi: 10.1007/s11630-022-1706-6.

[21] M. Sun and M. Zeng, "Investigation on turbulent flow and heat transfer characteristics and technical economy of corrugated tube," *Applied Thermal Engineering*, vol. 129, pp. 1–11, Jan. 2018, doi: 10.1016/j.applthermaleng.2017.09.136.

[22] F. W. Dittus and L. M. K. Boelter, "Heat transfer in automobile radiators of the tubular type," *International Communications in Heat and Mass Transfer*, vol. 12, no. 1, pp. 3–22, Jan. 1985, doi: 10.1016/0735-1933(85)90003-x.

[23] H. Blasius, "Das Aehnlichkeitsgesetz bei Reibungsvorgängen in Flüssigkeiten," in *Mitteilungen über Forschungsarbeiten auf dem Gebiete des Ingenieurwesens*, Berlin, Heidelberg: Springer Berlin Heidelberg, 1913, pp. 1–41. Accessed: Oct. 10, 2026. [Online]. Available: https://doi.org/10.1007/978-3-662-02239-9_1

[24] E. B. Ratts and A. G. Raut, "Entropy Generation Minimization of Fully Developed Internal Flow With Constant Heat Flux," *Journal of Heat Transfer*, vol. 126, no. 4, pp. 656–659, Jan. 2004, doi: 10.1115/1.1777585.